

Certified Finite-Shot Operating Windows for Virtual Distillation and Symmetry Verification

Vicenzo Scavino Alfaro

Independent researcher

June 12, 2026

Quantum error mitigation methods are often compared through infinite-shot bias, but real experiments are decided by finite sampling budgets, estimator instabilities, and per-shot resource costs. We develop a certified finite-shot operating-window theory for comparing virtual distillation (VD) and symmetry verification (SV). For each method we prove a mean-squared-error law with explicit non-asymptotic remainder constants, rather than only asymptotic delta-method statements. For VD, the law exposes the statistical bias and denominator instability of its quotient estimator and gives a concentration certificate for the sample size beyond which the quotient is trustworthy. For SV, it separates the residual bias floor left by undetectable errors from the sampling penalty set by the acceptance probability. These local laws feed into a selection trichotomy: any two-method comparison is a tie, a uniform dominance relation, or a genuine tradeoff with a certified crossing window and a self-consistency test that rejects spurious crossings. The theory makes falsifiable predictions—including operating-window locations scaling as p^{-2} or p^{-1} in the noise rate and the sign pattern of all pairwise comparisons. Exact white-box experiments confirm the predicted p^{-2} window scale with fitted exponent -1.97 and show 300/300 sign agreement within a pre-specified analysis; the single strict all-instance criterion that was not met is reported with its calibration analysis. Gate-level simulation and archived runs on two IBM backends then test the windows under device conditions: idealized VD windows exist, but realistic interferometry overhead and denominator instability move them outside the tested resource range, while calibrated SV has the lower MSE in the tested QAOA instances. The conclusion is therefore a regime statement, not a universal ranking: certified operating windows explain when a mitigation advantage should exist, when it should disappear, and which evidence validates coefficients rather than only device behavior.

1 Introduction

Quantum error mitigation (QEM) aims to improve observable estimates on noisy devices without implementing full fault tolerance [1]. Standard techniques include zero-noise extrapolation, probabilistic error cancellation, symmetry verification, Clifford-data regression, and multi-copy purification methods such as virtual distillation and error suppression by

Vicenzo Scavino Alfaro: u201919346@upc.edu.pe

derangements [2–15]. A common issue is that lower bias is not free. Mitigation can increase shot noise, circuit count, circuit width, calibration cost, or all of these.

We focus on two methods with analyzable finite-shot structure. Virtual distillation (VD) estimates an observable with respect to

$$\frac{\rho_p^M}{\text{Tr}(\rho_p^M)}, \quad (1)$$

where M noisy copies are combined [9, 10]. VD suppresses subdominant spectral components, but it cannot remove the mismatch between the dominant eigenvector of the noisy state and the ideal state [16]. Symmetry verification (SV) projects samples onto a valid symmetry sector and discards invalid samples [5, 6, 17, 18]. Its residual bias comes from symmetry-preserving errors that postselection cannot detect; its variance cost comes from the acceptance probability. Cai’s symmetry expansion framework already gives a broad bias-versus-sampling view for symmetry-based mitigation [19]. We use the narrower SV case as one component of an explicit operating-window theory.

The main mathematical issue is that VD is a quotient estimator. The population target is

$$\mu_{\text{VD},M}(p) = \frac{N_M(p)}{D_M(p)} = \frac{\text{Tr}(O\rho_p^M)}{\text{Tr}(\rho_p^M)}, \quad (2)$$

while the finite-shot estimator is \hat{N}_M/\hat{D}_M . Therefore a VD MSE law must account not only for population bias and variance, but also for the statistical bias of a random quotient and for the probability that the estimated denominator approaches zero. Prior VD analyses identify the population mechanism and noise floors [9, 10, 16], while circuit-level and hardware purification work studies implementation noise and special cases [20–22]. We place these effects inside a certified finite-budget MSE law. Operationally, the denominator certificate is a physical resolution condition: the copy-overlap signal D_M must be large enough, relative to the available shot budget and circuit cost, to be distinguished from sampling fluctuations before a VD advantage can be claimed.

The organizing thread of the paper is therefore simple. We first derive a local finite-shot law for each method, then certify the regime in which the law is valid, compare the resulting lower envelopes under a common resource budget, and finally test which parts of that certificate survive in simulation and hardware.

Our main finding is that neither method wins universally: the comparison is governed by operating windows whose location and scaling the theory predicts and certifies. In exact white-box experiments, the predicted p^{-2} window scale is recovered with fitted exponent -1.97 , and the predicted sign pattern of all pairwise method comparisons holds in 300/300 cells. Under gate-level device simulation and on archived IBM hardware, realistic interferometry overhead and denominator instability move the idealized VD window outside the tested resource range, and calibrated SV has the lower MSE in the tested QAOA instances—the same regime structure the windows predict. The device-level conclusion is not simply that VD needs more shots: the operating window predicted by the ideal law is displaced beyond the available physical resource budget once implementation costs are charged. Main results, assumptions, and limitations are stated in [Section 2](#).

Related finite-budget and threshold viewpoints are complementary. Shot-budget-aware regime identification has recently been explored for PEC in optimization benchmarking [23]; the operating windows here are certified at the level of non-asymptotic MSE laws and include the quotient-estimator structure of VD. Shot-estimation work for noisy circuits also separates statistical variance from a bias floor [24]; here that structure is used to compare

mitigation methods with explicit remainders and crossing certificates. Error-mitigation thresholds for imperfectly characterized random circuits address robustness to noise-model disorder [25], whereas our windows fix the transcript model and vary the sampling budget.

2 Main results and assumptions

The contribution is not a new heuristic benchmark, but a certified comparison framework. Its claims fall into seven connected parts.

1. **VD quotient law.** We derive the VD mean-squared-error law with explicit B^{-1} quotient bias and denominator-driven variance.
2. **VD residual bias.** We connect the VD bias-floor coefficient δ_{VD} directly to the first-order noise generator \mathcal{L} , the observable O , and the ideal pure state ρ_* .
3. **Denominator certificate.** We prove a concentration certificate showing when the VD quotient expansion is trustworthy.
4. **SV local law.** We give a precise first-order SV bias formula and separate variance-driven p/B dependence from quotient-bias terms, which vanish for Bernoulli postselection.
5. **Crossing validity.** We add a validity certificate for indifference curves, so a predicted crossing is accepted only when it falls inside the local-law regime.
6. **Decision-theoretic sanity check.** We prove a restricted lower bound: if two ideal targets induce physically indistinguishable noisy measurement transcripts at budget R , no mitigation selector can estimate both below the corresponding two-point risk.
7. **Selection structure.** We prove two structural organizing results that do not depend on numerical experiments: an accepted-transcript efficiency proposition for postselected laws and a selection trichotomy that organizes two-method comparisons into a degenerate tie, uniform dominance, or a genuine tradeoff whose crossing is certified under an explicit remainder condition.

We pair these mathematical claims with a tiered validation layer. Level 1 is the coefficient-checking layer: exact white-box density-matrix calculations compare the closed forms against ground truth, with the strict validation outcome reported separately in [Section 12](#). Levels 2 and 3 are not coefficient-validation layers. They test whether the finite-shot form, denominator concentration, crossing behavior, and implementation-overhead narrative remain visible under a Qiskit/Aer device model [26] and on IBM hardware with calibrated readout [27, 28].

The assumptions are local and method-specific. The noisy state is assumed to admit the first-order expansion in [Equation \(4\)](#); the VD dominant-eigenvector formula assumes a pure ideal output and a simple leading eigenvalue of ρ_p on the considered noise range, which is automatic near $p = 0$ for a pure ideal state; quotient certificates assume bounded one-shot numerator-denominator variables and an explicit denominator-concentration threshold; SV statements assume a fixed symmetry projector and report the residual undetectable-sector bias rather than claiming generic bias removal. We do not use the experimental layers to validate every analytic constant: Level 1 tests coefficient-level formulas, while Levels 2–3 test form, robustness, and operating-window behavior under device-model and hardware effects.

3 Problem setup and local laws

Let ρ_\star be the ideal output state and let $O = O^\dagger$ be a bounded observable. The target is

$$\mu_\star = \text{Tr}(O\rho_\star). \quad (3)$$

The noisy output state at physical noise scale $p \geq 0$ is ρ_p . We assume the local expansion

$$\rho_p = \rho_\star + p\Delta + \mathcal{O}(p^2), \quad \Delta = \mathcal{L}(\rho_\star), \quad (4)$$

where $\Delta = \Delta^\dagger$ and $\text{Tr} \Delta = 0$. The $\mathcal{O}(p^2)$ term is in any fixed matrix norm; all Hilbert spaces considered here are finite-dimensional. The trace condition follows from $\text{Tr} \rho_p = 1$.

A mitigation method m produces an estimator $\hat{\mu}_m$. Its performance is

$$\text{MSE}_m(p, B) = \mathbb{E}[(\hat{\mu}_m - \mu_\star)^2] = \text{Bias}(\hat{\mu}_m)^2 + \text{Var}(\hat{\mu}_m), \quad (5)$$

where B denotes the number of independent statistical samples for that method.

Definition 1 (Certified local finite-shot law). *A method m has a certified local finite-shot law on a parameter set \mathcal{P} if there exist functions $b_m(p)$, $v_m(p)$, $c_m(p)$, constants $C_m(p)$, and a threshold $B_{\min, m}(p)$ such that, for every $p \in \mathcal{P}$ and $B \geq B_{\min, m}(p)$,*

$$\text{MSE}_m(p, B) = b_m(p)^2 + \frac{v_m(p) + 2b_m(p)c_m(p)}{B} + \rho_m(p, B), \quad |\rho_m(p, B)| \leq \frac{C_m(p)}{B^2}. \quad (6)$$

We write $\tilde{v}_m(p) = v_m(p) + 2b_m(p)c_m(p)$. This is the leading $1/B$ coefficient of the MSE, not necessarily a pure variance coefficient; when $b_m c_m < 0$, the quotient-bias cross-term can reduce the local slope. The finite-sample bias coefficient c_m is the same ratio-estimator effect familiar in survey sampling [29]. The crossing theorems below keep the relevant sign conditions explicit rather than assuming $\tilde{v}_m \geq 0$. Some ratio estimators first produce a two-part bound

$$|\rho_m(p, B)| \leq \frac{C_m(p)}{B^2} + C_m^{\text{exp}}(p)e^{-\gamma_m(p)B}, \quad \gamma_m(p) > 0. \quad (7)$$

Such a statement is converted into Equation (6) by increasing the threshold to any $B_{\text{exp}, m}(p)$ satisfying

$$B_{\text{exp}, m}(p) \geq \frac{2}{\gamma_m(p)}, \quad C_m^{\text{exp}}(p)e^{-\gamma_m(p)B_{\text{exp}, m}(p)} \leq \frac{C_{m, \text{abs}}(p)}{B_{\text{exp}, m}(p)^2}, \quad (8)$$

and replacing C_m by $C_m + C_{m, \text{abs}}$. Since $B^2 e^{-\gamma_m(p)B}$ is decreasing for $B \geq 2/\gamma_m(p)$, this absorption then holds for every $B \geq B_{\text{exp}, m}(p)$. Thus exponential bad-denominator terms are not silently hidden in the local law; they are either displayed explicitly or absorbed after an explicit sample-size threshold.

The cross-term $2b_m c_m/B$ is retained because it is the leading interaction between population bias and statistical quotient bias. When a method is a plain sample mean, $c_m = 0$. When the leading MSE coefficient $\tilde{v}_m(p)$ depends smoothly on p , the local expansion of $\tilde{v}_m(p)/B$ generally contains p/B terms. Those terms should not be hidden inside $\mathcal{O}(p^2/B)$ unless the first derivative vanishes.

For unmitigated estimation,

$$\mu_0(p) = \text{Tr}(O\rho_p), \quad b_0(p) = \mu_0(p) - \mu_\star = \beta_0 p + \mathcal{O}(p^2), \quad \beta_0 = \text{Tr}(O\Delta). \quad (9)$$

If the one-shot variance is $\sigma_0^2(p)$, then

$$\text{MSE}_0(p, B) = b_0(p)^2 + \frac{\sigma_0^2(p)}{B}. \quad (10)$$

4 Virtual distillation: population law

For $M \geq 2$, idealized VD targets

$$\mu_{\text{VD},M}(p) = \frac{N_M(p)}{D_M(p)}, \quad N_M(p) = \text{Tr}(O\rho_p^M), \quad D_M(p) = \text{Tr}(\rho_p^M). \quad (11)$$

Assume the spectral decomposition

$$\rho_p = \sum_{j \geq 1} \lambda_j(p) |\phi_j(p)\rangle \langle \phi_j(p)|, \quad \lambda_1(p) > \lambda_2(p) \geq \dots \geq 0. \quad (12)$$

Then

$$\mu_{\text{VD},M}(p) = \frac{\sum_j \lambda_j(p)^M O_{jj}(p)}{\sum_j \lambda_j(p)^M}, \quad O_{jj}(p) = \langle \phi_j(p) | O | \phi_j(p) \rangle. \quad (13)$$

VD suppresses the subdominant eigenvalues, but it converges to the observable expectation in the dominant eigenvector:

$$\lim_{M \rightarrow \infty} \mu_{\text{VD},M}(p) = O_{11}(p). \quad (14)$$

The infinite-copy floor is therefore

$$b_{\text{VD},\infty}(p) = O_{11}(p) - \mu_\star. \quad (15)$$

Lemma 1 (Spectral leakage). *Let*

$$r_M(p) = \sum_{j > 1} \left(\frac{\lambda_j(p)}{\lambda_1(p)} \right)^M. \quad (16)$$

Then

$$|\mu_{\text{VD},M}(p) - O_{11}(p)| \leq \frac{2 \|O\|_\infty r_M(p)}{1 + r_M(p)} \leq 2 \|O\|_\infty r_M(p). \quad (17)$$

Proof. Divide numerator and denominator by λ_1^M . The difference from O_{11} is a weighted average of $O_{jj} - O_{11}$ over $j > 1$, divided by $1 + r_M$. Since $|O_{jj} - O_{11}| \leq 2 \|O\|_\infty$, the bound follows. \square

4.1 First-order endpoint coefficient in terms of the noise generator

Assume now that $\rho_\star = |\psi_\star\rangle \langle \psi_\star|$ is pure. Let

$$Q_\star = I - |\psi_\star\rangle \langle \psi_\star|. \quad (18)$$

The eigenvalue 1 of ρ_\star is simple and separated from the zero eigenspace by a unit gap. The $\mathcal{O}(p^2)$ operator term in Equation (4) changes the dominant eigenvector only at order $\mathcal{O}(p^2)$ by this unit gap. Standard non-degenerate eigenvector perturbation [30] gives

$$|\phi_1(p)\rangle = |\psi_\star\rangle + p |\eta\rangle + \mathcal{O}(p^2), \quad |\eta\rangle = Q_\star \Delta |\psi_\star\rangle, \quad \langle \psi_\star | \eta \rangle = 0. \quad (19)$$

Proposition 1 (VD floor coefficient). *Under Equation (4) and Equation (19),*

$$b_{\text{VD},\infty}(p) = \delta_{\text{VD}} p + \mathcal{O}(p^2), \quad (20)$$

with

$$\delta_{\text{VD}} = 2 \text{Re} \langle \psi_\star | O Q_\star \Delta |\psi_\star\rangle = 2 \text{Re} \langle \psi_\star | O (I - |\psi_\star\rangle \langle \psi_\star|) \mathcal{L}(\rho_\star) |\psi_\star\rangle. \quad (21)$$

Proof. By expansion of the dominant eigenvector,

$$O_{11}(p) = \langle \psi_\star + p\eta | O | \psi_\star + p\eta \rangle + \mathcal{O}(p^2) \quad (22)$$

$$= \mu_\star + 2p \operatorname{Re} \langle \psi_\star | O | \eta \rangle + \mathcal{O}(p^2). \quad (23)$$

Substitute $|\eta\rangle = Q_\star \Delta |\psi_\star\rangle$. □

The same first-order coefficient holds for every fixed finite copy number $M \geq 2$. Indeed, Weyl continuity [31] applied to $\rho_p = \rho_\star + \mathcal{O}(p)$ gives $\lambda_1(p) = 1 + \mathcal{O}(p)$ and $\lambda_j(p) = \mathcal{O}(p)$ for $j > 1$, so $r_M(p) = \mathcal{O}(p^M)$. By Lemma 1, $\mu_{\text{VD},M}(p) - O_{11}(p) = \mathcal{O}(p^M) = \mathcal{O}(p^2)$ for $M \geq 2$, and therefore

$$b_{\text{VD},M}(p) = \delta_{\text{VD}} p + \mathcal{O}(p^2), \quad M \geq 2 \text{ fixed.} \quad (24)$$

This formula prevents δ_{VD} from being a free symbol: it is the local first-order form of the dominant-eigenvector mismatch identified in Koczor [16], written directly as an observable-dependent projection of the first-order noise perturbation onto the orthogonal subspace of the ideal state.

5 Virtual distillation: denominator concentration and quotient MSE

Let $(X_{M,s}, Y_{M,s})_{s=1}^B$ be independent copies of a one-sample pair satisfying

$$\mathbb{E}X_M = N_M(p), \quad \mathbb{E}Y_M = D_M(p), \quad (25)$$

and define

$$\hat{N}_M = \frac{1}{B} \sum_{s=1}^B X_{M,s}, \quad \hat{D}_M = \frac{1}{B} \sum_{s=1}^B Y_{M,s}, \quad \hat{\mu}_{\text{VD},M} = \frac{\hat{N}_M}{\hat{D}_M}. \quad (26)$$

Write $\sigma_{N,M}^2(p) = \operatorname{Var}(X_M)$, $\sigma_{D,M}^2(p) = \operatorname{Var}(Y_M)$, and $\sigma_{ND,M}(p) = \operatorname{Cov}(X_M, Y_M)$ for the one-shot variance and covariance coefficients used in the quotient law below. The ratio is meaningful only when the denominator is statistically separated from zero. This point is part of the operating-window theory, not a technical nuisance.

Assumption 1 (Bounded one-shot VD estimator). *For fixed (p, M) , $D_M(p) > 0$, and the numerator-denominator one-shot pair satisfies*

$$|X_M| \leq K_{N,M}(p), \quad |Y_M - D_M(p)| \leq K_{D,M}(p) \quad (27)$$

almost surely. Define centered variables $\xi = X_M - N_M$ and $\zeta = Y_M - D_M$, and signed one-shot moment constants

$$m_{ab,M}(p) = \mathbb{E}[\xi^a \zeta^b]. \quad (28)$$

Lemma 2 (Bernstein denominator certificate). *Under Assumption 1,*

$$\mathbb{P}\left(\left|\hat{D}_M - D_M\right| \geq \frac{D_M}{2}\right) \leq 2 \exp\left[-\frac{BD_M(p)^2}{8\sigma_{D,M}^2(p) + \frac{4}{3}K_{D,M}(p)D_M(p)}\right]. \quad (29)$$

Consequently, to make this bilateral bad-denominator probability at most ε , it is sufficient that

$$B \geq B_{\text{den},M}(p, \varepsilon) := \left(\frac{8\sigma_{D,M}^2(p)}{D_M(p)^2} + \frac{4K_{D,M}(p)}{3D_M(p)}\right) \log \frac{2}{\varepsilon}. \quad (30)$$

Proof. Apply Bernstein's inequality to both tails of $B^{-1} \sum_s (Y_{M,s} - D_M)$ with threshold $D_M/2$, and take a union bound [32]. \square

The ratio $\sigma_{D,M}^2/D_M^2$ in Equation (30) is the denominator-driven inflation parameter. If D_M is small, VD may still have a favorable population bias but require many samples before the ratio estimator is stable.

For a non-asymptotic statement define the clipped quotient

$$\hat{\mu}_{\text{VD},M}^{\text{clip}} = \frac{\hat{N}_M}{\max\{\hat{D}_M, D_M/2\}}. \quad (31)$$

It equals the ordinary quotient on the good event $\hat{D}_M \geq D_M/2$. The clipping is a proof device; in practice it is also the natural regularization when a random denominator is used. The same proof works with any known floor $\tau \in (0, D_M/2]$, with τ -dependent constants; the choice $D_M/2$ gives the cleanest certificate.

The certificate is stated in terms of explicit one-shot moment envelopes. Definition 2 in Section B assembles, from the bounded pair of Assumption 1, finite moment envelopes $\mathfrak{m}_{ab,M}(p)$, expectation- and variance-remainder constants $A_{E,M}(p)$ and $A_{V,M}(p)$, bad-event prefactors $B_{E,M}(p)$ and $B_{V,M}(p) = 2B_{E,M}(p)^2$, and the exponential bad-event term $E_{\text{bad},M}(p, B)$; the ratio $\omega_M(p) = K_{D,M}(p)/D_M(p)$ controls the bad-event bookkeeping. Only these roles are needed to read the theorem below; the full assembly is displayed in Section B. The classical delta-method form of the leading coefficients is recalled in Section A.

Remark 1 (Tightness of the certified constants). *The constants in Equation (B.11) are proof certificates, not sharp estimates of the physical sampling penalty. The main looseness comes from the crude bounded-sign envelope for $\mathfrak{t}_M^{(V)}$, the event-local bad-denominator sup-norms, and the fourth-moment envelopes used in $A_{E,M}$ and $A_{Q,M}$. These steps are robust by design but can overestimate the true second moment by several orders of magnitude. Consequently, the small numerical parameters used in the toy non-vacuity checks below are artifacts of a loose variance certificate, not physical thresholds. The Efron–Stein certificate in Lemma 3 and the direct second-order calculation in Proposition B.1 are included precisely to separate what is needed for a rigorous certificate from what is expected to control the true sampling scale. In the validation layer, the Level 1 white-box simulations provide the sharper empirical sampling scale against the exact closed forms; those numerical scales soften the practical reading of the extreme toy parameters, but they do not replace the certified constants in the theorem statements.*

Theorem 1 (Non-asymptotic VD quotient law with explicit moment remainder). *Under Assumption 1, for every $B \geq 1$, the clipped VD estimator satisfies*

$$\mathbb{E}[\hat{\mu}_{\text{VD},M}^{\text{clip}}] = \mu_{\text{VD},M}(p) + \frac{c_{\text{VD},M}(p)}{B} + r_M^{(E)}(p, B), \quad (32)$$

$$\text{Var}(\hat{\mu}_{\text{VD},M}^{\text{clip}}) = \frac{v_{\text{VD},M}(p)}{B} + r_M^{(V)}(p, B), \quad (33)$$

where

$$c_{\text{VD},M}(p) = \frac{\mu_{\text{VD},M}(p)\sigma_{D,M}^2(p) - \sigma_{ND,M}(p)}{D_M(p)^2}, \quad (34)$$

$$v_{\text{VD},M}(p) = \frac{\sigma_{N,M}^2(p) + \mu_{\text{VD},M}(p)^2\sigma_{D,M}^2(p) - 2\mu_{\text{VD},M}(p)\sigma_{ND,M}(p)}{D_M(p)^2} \quad (35)$$

$$= \frac{\text{Var}(X_M - \mu_{\text{VD},M}(p)Y_M)}{D_M(p)^2}. \quad (36)$$

Moreover,

$$\left| r_M^{(E)}(p, B) \right| \leq \frac{A_{E,M}(p)}{B^2} + B_{E,M}(p) \exp \left[-\frac{BD_M(p)^2}{8\sigma_{D,M}^2(p) + \frac{4}{3}K_{D,M}(p)D_M(p)} \right], \quad (37)$$

$$\left| r_M^{(V)}(p, B) \right| \leq \frac{A_{V,M}(p)}{B^2} + E_{\text{bad},M}(p, B). \quad (38)$$

Therefore

$$\text{MSE}_{\text{VD},M}(p, B) = b_{\text{VD},M}(p)^2 + \frac{v_{\text{VD},M}(p) + 2b_{\text{VD},M}(p)c_{\text{VD},M}(p)}{B} + \rho_{\text{VD},M}(p, B), \quad (39)$$

where $b_{\text{VD},M}(p) := \mu_{\text{VD},M}(p) - \mu_\star$. The constants $B_{E,M}$ and $B_{V,M}$ are those in [Definition 2](#). The remainder obeys

$$|\rho_{\text{VD},M}(p, B)| \leq \frac{C_{\text{VD},M}(p)}{B^2} + C'_{\text{VD},M}(p) \exp \left[-\frac{BD_M(p)^2}{8\sigma_{D,M}^2(p) + \frac{4}{3}K_{D,M}(p)D_M(p)} \right], \quad (40)$$

where one admissible explicit choice is

$$C_{\text{VD},M} = A_{V,M} + c_{\text{VD},M}^2 + 2|b_{\text{VD},M}|A_{E,M} + 2|c_{\text{VD},M}|A_{E,M} + 2A_{E,M}^2, \quad (41)$$

$$C'_{\text{VD},M} = B_{V,M} + 2|b_{\text{VD},M}|B_{E,M} + 2|c_{\text{VD},M}|B_{E,M} + 2B_{E,M}^2. \quad (42)$$

These constants are not optimized; they are written only to make the certificate reproducible. In the strict sense of [Definition 1](#), choose any $B_{\text{exp,VD},M}$ satisfying [Equation \(8\)](#) with

$$\gamma_{\text{VD},M}(p) = \frac{D_M(p)^2}{8\sigma_{D,M}^2(p) + \frac{4}{3}K_{D,M}(p)D_M(p)}, \quad C_{\text{VD},M}^{\text{exp}}(p) = C'_{\text{VD},M}(p), \quad (43)$$

and absorb the exponential contribution into the B^{-2} remainder whenever

$$B \geq B_{\text{exp,VD},M}.$$

The denominator scale $B_{\text{den},M}(p, \varepsilon)$ in [Equation \(30\)](#) is the optional high-probability scale that makes $\mathbb{P}(G^c) \leq \varepsilon$; it is not needed for the displayed exponential inequalities, which hold for every $B \geq 1$.

Proof in [Section C](#).

Remark 2 (Ordinary versus clipped quotient). *If the implementation guarantees the needed inverse-moment control for \widehat{D}_M^{-1} , the same leading expansion applies to the ordinary quotient. Without such a guarantee, the clipped quotient is the mathematically safe estimator. The two estimators coincide on $\{\widehat{D}_M \geq D_M/2\}$, so their leading operating-window laws agree whenever the ordinary quotient has controlled tails on the complementary event. For sign-valued denominator streams, $\widehat{D}_M = 0$ can occur with positive probability for some finite B unless the distribution is degenerate; in that case a floor or clipping rule is required before the finite-sample MSE is a well-defined certified object.*

5.1 Sharper variance diagnostics for the VD quotient

The certified law above is worst-case by construction. We add a sharper, fully non-asymptotic Efron–Stein certificate for the total variance of the clipped quotient. It does not recover the exact coefficient $v_{\text{VD},M}$, but it avoids the large bounded-moment remainder envelope used in $A_{V,M}$. A complementary asymptotic second-order variance calculation, which identifies the moment combination controlling the true B^{-2} correction, is given in [Proposition B.1](#) in [Section B](#).

Lemma 3 (Efron–Stein total-variance certificate for clipped VD). *Under [Assumption 1](#), the clipped quotient in [Equation \(31\)](#) satisfies*

$$\text{Var}\left(\widehat{\mu}_{\text{VD},M}^{\text{clip}}\right) \leq \frac{8K_{N,M}^2(D_M + 2K_{D,M})^2}{D_M^4} \frac{1}{B}. \quad (44)$$

Consequently, for $D_M \geq 1/2$ and bounded Hadamard-test signs $K_{N,M}, K_{D,M} = \mathcal{O}(1)$, the clipped VD quotient has a non-asymptotic total-variance certificate with a constant often of order 10^2 – 10^3 in the bounded-sign cases considered below, rather than the much larger B^{-2} -remainder envelope in [Equation \(B.11\)](#).

Proof. Let f be the clipped quotient as a function of the B independent pairs (X_s, Y_s) . Replace only the j -th pair and denote the resulting function by $f^{(j)}$. The sample numerator changes by at most $2K_{N,M}/B$, while the sample denominator changes by at most $2K_{D,M}/B$. Since the clipped denominator is always at least $D_M/2$, the map $(n, d) \mapsto n/\max\{d, D_M/2\}$ is Lipschitz with constants $2/D_M$ in n and at most $4K_{N,M}/D_M^2$ in d , using $|\widehat{N}_M| \leq K_{N,M}$. Hence

$$|f - f^{(j)}| \leq \frac{4K_{N,M}}{BD_M} + \frac{8K_{N,M}K_{D,M}}{BD_M^2} = \frac{4K_{N,M}(D_M + 2K_{D,M})}{BD_M^2}. \quad (45)$$

The Efron–Stein inequality [\[32\]](#) gives

$$\text{Var}(f) \leq \frac{1}{2} \sum_{j=1}^B \mathbb{E}[(f - f^{(j)})^2] \leq \frac{B}{2} \left(\frac{4K_{N,M}(D_M + 2K_{D,M})}{BD_M^2} \right)^2, \quad (46)$$

which is [Equation \(44\)](#). □

6 Copy-number choice for VD

The copy number M is not a free improvement knob. Increasing M suppresses subdominant spectral components, but it can also reduce $D_M = \text{Tr}(\rho_p^M)$, which increases the denominator-driven variance.

Lemma 4 (Denominator spectral bounds). *Let $r_M(p) = \sum_{j>1} (\lambda_j/\lambda_1)^M$. Then*

$$D_M(p) = \lambda_1(p)^M (1 + r_M(p)), \quad \lambda_1(p)^M \leq D_M(p). \quad (47)$$

Proof. Use $D_M = \sum_j \lambda_j^M$ and factor out λ_1^M . □

6.1 Concrete independent derangement/Hadamard-test implementation

To anchor the variance constants in a concrete implementation, we fix the following idealized estimator. Let U_M be the cyclic derangement acting on M copies. The denominator $D_M = \text{Tr}(\rho_p^M)$ is estimated by a controlled- U_M Hadamard test [33]. For a Pauli observable O , the numerator $N_M = \text{Tr}(O\rho_p^M)$ is estimated by an independent controlled observable-derangement Hadamard test. Indeed, the observable-derangement operator is a product of a Pauli unitary and U_M , hence unitary, so the standard Hadamard test applies. Each test returns a binary outcome in $\{\pm 1\}$. We use B denominator shots and B numerator shots; hence the physical resource is proportional to $R_M = 2\kappa_M B$, where κ_M is the circuit resource per Hadamard test.

For this implementation,

$$X_M \in \{\pm 1\}, \quad Y_M \in \{\pm 1\}, \quad \mathbb{E}X_M = N_M, \quad \mathbb{E}Y_M = D_M, \quad (48)$$

and the two streams are independent. Therefore

$$\sigma_{N,M}^2 = 1 - N_M^2, \quad \sigma_{D,M}^2 = 1 - D_M^2, \quad \sigma_{ND,M} = 0. \quad (49)$$

The VD quotient constants become

$$c_{\text{VD},M}^{\text{Had}}(p) = \frac{\mu_{\text{VD},M}(p)(1 - D_M(p)^2)}{D_M(p)^2}, \quad (50)$$

$$v_{\text{VD},M}^{\text{Had}}(p) = \frac{1 - N_M(p)^2 + \mu_{\text{VD},M}(p)^2(1 - D_M(p)^2)}{D_M(p)^2}. \quad (51)$$

For Pauli O with $\|O\|_\infty \leq 1$, positivity of ρ_p^M gives $|N_M| \leq \text{Tr}(\rho_p^M) = D_M$, hence $|\mu_{\text{VD},M}| \leq 1$. The denominator certificate is explicit:

$$B \geq \left(\frac{8(1 - D_M^2)}{D_M^2} + \frac{8}{3D_M} \right) \log \frac{2}{\varepsilon} \quad (52)$$

is sufficient for $\mathbb{P}(|\hat{D}_M - D_M| \geq D_M/2) \leq \varepsilon$.

Remark 3 (One-sided operational convention for B_{den}). *The event monitored by the numerical diagnostics in this work is the one-sided clip event $\{\hat{D}_M < D_M/2\}$, for which the one-sided Bernstein bound holds without the bilateral prefactor 2:*

$$\mathbb{P}\left(\hat{D}_M < \frac{D_M}{2}\right) \leq \exp\left[-\frac{BD_M(p)^2}{8\sigma_{D,M}^2(p) + \frac{4}{3}K_{D,M}(p)D_M(p)}\right]. \quad (53)$$

Accordingly, every B_{den} value and B/B_{den} coordinate reported in the Level 1–3 diagnostics uses the one-sided threshold obtained from Equation (30) (equivalently Equation (52)) by replacing $\log(2/\varepsilon)$ with $\log(1/\varepsilon)$, evaluated at $\varepsilon = 10^{-3}$; at $B = B_{\text{den}}$ the one-sided bound Equation (53) then equals ε exactly. The one-sided threshold coincides with the bilateral $B_{\text{den},M}(p, \varepsilon)$ evaluated at failure probability 2ε , and is smaller than the bilateral threshold at the same ε by the factor $\log(1/\varepsilon)/\log(2/\varepsilon) \simeq 0.91$ for $\varepsilon = 10^{-3}$. The ‘‘Bernstein bound’’ curves in the Level 2 denominator figure are likewise the one-sided bound Equation (53).

Proposition 2 (VD implementation variance inflation). *For the independent Hadamard-test implementation above,*

$$v_{\text{VD},M}^{\text{Had}}(p) \leq \frac{2}{D_M(p)^2} \leq 2\lambda_1(p)^{-2M}. \quad (54)$$

If, in addition, $1 - N_M(p)^2 \geq v_- > 0$ on the considered parameter range, then

$$v_{\text{VD},M}^{\text{Had}}(p) \geq v_- \lambda_1(p)^{-2M} (1 + r_M(p))^{-2}. \quad (55)$$

Proof. The upper bound follows from Equation (51) and $D_M \geq \lambda_1^M$. The lower bound uses the numerator-variance term $(1 - N_M^2)/D_M^2$ and $D_M = \lambda_1^M(1 + r_M)$. \square

The next proposition is a model-dependent refinement rather than a compiled-circuit noise theorem; Remark 4 states its intended scope.

Proposition 3 (Multiplicative implementation-noise shift of the VD law). *Suppose the controlled-derangement/Hadamard tests used to estimate the population quantities are followed by effective sign contractions*

$$\tilde{N}_M = \eta_{N,M} N_M, \quad \tilde{D}_M = \eta_{D,M} D_M, \quad \eta_{N,M}, \eta_{D,M} > 0, \quad (56)$$

with $\theta_M^{\text{impl}} := \eta_{N,M}/\eta_{D,M}$. Then the implemented population quotient is

$$\mu_{\text{VD},M}^{\text{impl}} = \theta_M^{\text{impl}} \frac{N_M}{D_M}, \quad (57)$$

so the implemented population bias is

$$b_{\text{VD},M}^{\text{impl}} = \left(\theta_M^{\text{impl}} - 1 \right) \frac{N_M}{D_M} + b_{\text{VD},M}. \quad (58)$$

If the same contraction affects numerator and denominator, $\theta_M^{\text{impl}} = 1$, the population quotient is unchanged and implementation noise appears first as sampling inflation. In the independent sign model with one-shot variables in $\{\pm 1\}$,

$$v_{\text{VD},M}^{\text{impl}} = \frac{1 - \eta_{N,M}^2 N_M^2 + (\theta_M^{\text{impl}} N_M / D_M)^2 (1 - \eta_{D,M}^2 D_M^2)}{\eta_{D,M}^2 D_M^2}. \quad (59)$$

Consequently, in the common-contraction case $\eta_{N,M} = \eta_{D,M} = \eta_M$, the population quotient and hence the bias gap are unchanged. The denominator part of the sampling coefficient carries an η_M^{-2} -type inflation, but the full coefficient is not generally a pure multiplicative rescaling of the ideal one because the Bernoulli variances are also replaced by $1 - \eta_M^2 N_M^2$ and $1 - \eta_M^2 D_M^2$.

Proof. The first two displays follow by taking the ratio of the contracted means. For the variance coefficient, substitute the contracted means into the quotient variance formula Equation (35) with independent numerator and denominator signs, so the covariance term is zero. The denominator in Equation (35) becomes $(\eta_{D,M} D_M)^2$, giving Equation (59). If $\eta_{N,M} = \eta_{D,M} = \eta_M$, then the population quotient and hence the bias gap are unchanged. The denominator in the quotient-variance formula contributes an η_M^{-2} -type inflation, but Equation (59) also replaces the Bernoulli variance factors by $1 - \eta_M^2 N_M^2$ and $1 - \eta_M^2 D_M^2$. Thus the leading crossing budget should be computed from the displayed coefficient rather than by applying a universal scalar multiplier to the ideal variance. \square

Remark 4 (Interpretation). *This model records the algebraic effect of multiplicative read-out or controlled-test contractions on a VD quotient. It is narrower than a circuit-level noise analysis: a compiled derangement implementation may create correlated numerator-denominator errors, coherent control errors, or nonmultiplicative distortions. The proposition is a falsifiable baseline for the experimental section: common multiplicative test noise cancels in the population ratio but modifies the sampling coefficient through Equation (59); asymmetric test noise creates an additional first-order bias.*

Theorem 2 (Logarithmic copy-number scale for implemented VD). *Fix p and suppose that, for M in an admissible range before the dominant-eigenvector floor takes over,*

$$A_-^2 q^{2M} \leq (b_{\text{VD},M}(p) - b_{\text{VD},\infty}(p))^2 \leq A_+^2 q^{2M}, \quad q = \frac{\lambda_2(p)}{\lambda_1(p)} < 1, \quad 0 < \lambda_2(p) < \lambda_1(p), \quad (60)$$

and the Hadamard-test variance has the two-sided scaling in Proposition 2. Then every minimizer of the leading implemented VD objective

$$\mathcal{E}_M(B) = A^2 q^{2M} + \frac{V \lambda_1^{-2M}}{B} \quad (61)$$

lies within an $\mathcal{O}(1)$ additive distance of

$$M_B = \frac{\log B}{2 |\log \lambda_2(p)|}. \quad (62)$$

Since $\lambda_1(p) = 1 + \mathcal{O}(p)$ in the local pure-state regime,

$$M_B = \Theta \left(\frac{\log B}{|\log(\lambda_2(p)/\lambda_1(p))|} \right) \quad (63)$$

up to local λ_1 -dependent constants. The objective \mathcal{E}_M is the M -dependent part of the leading MSE in the admissible range: there $|b_{\text{VD},\infty}| \lesssim q^M$, so the cross-term $2b_{\text{VD},\infty}(b_{\text{VD},M} - b_{\text{VD},\infty})$ is absorbed into the constant multiplying q^{2M} . Once $|b_{\text{VD},\infty}|$ is comparable to the leakage term, the optimal copy number saturates because additional copies increase variance without reducing the floor.

Proof. Balance the decreasing leakage term against the increasing denominator-driven variance term:

$$q^{2M} \asymp B^{-1} \lambda_1^{-2M}. \quad (64)$$

Equivalently, $(q\lambda_1)^{2M} \asymp B^{-1}$. Since $q\lambda_1 = \lambda_2$, Equation (62) follows. The two-sided constants in Equation (60) and Proposition 2 shift the minimizer only by an additive constant independent of B . Integer rounding also changes M by at most a constant. \square

Remark 5. *The exact logarithmic denominator contains $|\log \lambda_2|$, because the variance inflation is driven by $D_M \sim \lambda_1^M$ while leakage is driven by $(\lambda_2/\lambda_1)^M$. In the small-noise regime $\lambda_1 \approx 1$, this is equivalent to the more informal $\log B / |\log(\lambda_2/\lambda_1)|$ scaling. This distinction matters because it identifies which part of VD controls the cost.*

7 Symmetry verification

Let P be the projector onto the valid symmetry sector and assume

$$P \rho_\star P = \rho_\star. \quad (65)$$

For a symmetry-compatible observable, SV estimates

$$\mu_{\text{SV}}(p) = \frac{\text{Tr}(OP\rho_pP)}{a(p)}, \quad a(p) = \text{Tr}(P\rho_p). \quad (66)$$

The first-order projected state is

$$\frac{P\rho_pP}{\text{Tr}(P\rho_p)} = \rho_\star + p(P\Delta P - \rho_\star \text{Tr}(P\Delta P)) + \mathcal{O}(p^2). \quad (67)$$

A precise detectable-undetectable split can be defined by

$$\Delta_{\text{undet}} = P\Delta P, \quad P\Delta_{\text{det}}P = 0, \quad \Delta = \Delta_{\text{undet}} + \Delta_{\text{det}} \quad (68)$$

with $\Delta_{\text{det}} = \Delta - P\Delta P$ for this first-order analysis. The split is canonical once P is fixed: the detectable part is exactly the part that has no component inside the postselected block.

Proposition 4 (SV first-order bias). *Under Equation (4) and $P\rho_{\star}P = \rho_{\star}$,*

$$a(p) = 1 + p \text{Tr}(P\Delta) + \mathcal{O}(p^2), \quad (69)$$

and

$$b_{\text{SV}}(p) = \mu_{\text{SV}}(p) - \mu_{\star} = \delta_{\text{SV}}p + \mathcal{O}(p^2), \quad (70)$$

where

$$\delta_{\text{SV}} = \text{Tr}(OP\Delta P) - \mu_{\star} \text{Tr}(P\Delta P). \quad (71)$$

If one writes $a(p) = 1 - \alpha_{\text{det}}p + \mathcal{O}(p^2)$, then $\alpha_{\text{det}} = -\text{Tr}(P\Delta)$.

Proof. Use $P\rho_pP = \rho_{\star} + pP\Delta P + \mathcal{O}(p^2)$ and

$$\frac{1}{1 + p \text{Tr}(P\Delta P) + \mathcal{O}(p^2)} = 1 - p \text{Tr}(P\Delta P) + \mathcal{O}(p^2). \quad (72)$$

Substitute into $\text{Tr}(OP\rho_pP)/\text{Tr}(P\rho_pP)$ and subtract μ_{\star} . \square

Remark 6 (Depolarizing noise carries no first-order SV bias in a fixed sector). *Let P project onto a fixed Hamming-weight sector, let O be Z -diagonal with $[O, P] = 0$, and let $P\rho_{\star}P = \rho_{\star}$. For single-qubit depolarizing noise with arbitrary per-qubit rates c_i , the generator is $\Delta = \sum_i c_i [(I_i/2) \otimes \text{Tr}_i \rho_{\star} - \rho_{\star}]$. For a basis string z inside the sector, the diagonal entry of $(I_i/2) \otimes \text{Tr}_i \rho_{\star}$ at z is $\frac{1}{2}[q(z^{i \rightarrow 0}) + q(z^{i \rightarrow 1})] = \frac{1}{2}q(z)$, where q is the (sector-supported) diagonal of ρ_{\star} : flipping bit i moves z out of the sector, so only the z -term survives. Inside the sector the replacement term is therefore proportional to the diagonal of ρ_{\star} itself, and since only diagonals enter traces against the diagonal O and P , $\delta_{\text{SV}} = \sum_i c_i [(\frac{1}{2}\mu_{\star} - \mu_{\star}\frac{1}{2}) - (\mu_{\star} - \mu_{\star})] = 0$ identically. No centering or trace condition on O is required: the subtraction $-\mu_{\star} \text{Tr}(P\Delta P)$ built into δ_{SV} cancels any component of $P\Delta P$ proportional to ρ_{\star} automatically. The diagonality of O is essential, however, not cosmetic: inside the sector, $(I_i/2) \otimes \text{Tr}_i \rho_{\star}$ matches $\frac{1}{2}\rho_{\star}$ only on the diagonal—coherences between sector strings differing at bit i are dephased—so the cancellation is not claimed for general symmetry-compatible observables. Thus a first-order SV bias floor requires sector-preserving structured noise—such as the heterogeneous amplitude-damping component of the fixed channel—whereas the sector-preserving residue of depolarizing noise is proportional to the ideal state and leaves the postselected expectation unbiased at first order. This zero-bias statement is therefore not a hardware-noise assumption: T_1/T_2 -type channels, amplitude-damping components, coherent calibration errors, or other inhomogeneous sector-preserving components can produce a nonzero projected generator $P\Delta P - \rho_{\star} \text{Tr}(P\Delta P)$, and must be evaluated through Equation (71). The pre-specified channel-sensitivity check in Section 12 confirms only the depolarizing cancellation to machine precision on the fixed ensemble.*

Let $A_s \in \{0, 1\}$ be the acceptance indicator and W_s the measured value when accepted. Put $Z_s = A_s W_s$. Then

$$\hat{\mu}_{\text{SV}} = \frac{\bar{Z}}{A}, \quad \mathbb{E}A = a(p), \quad \mathbb{E}Z = a(p)\mu_{\text{SV}}(p). \quad (73)$$

Theorem 3 (Certified SV postselection quotient law). *Assume $a(p) > 0$, $A \in \{0, 1\}$, and $|W| \leq K_W$ on accepted shots. Put $Z = AW$, $\mu_{\text{SV}} = \mathbb{E}Z/a$, and define centered variables*

$$\xi_{\text{SV}} = Z - a\mu_{\text{SV}}, \quad \zeta_{\text{SV}} = A - a. \quad (74)$$

Let $\hat{\mu}_{\text{SV}}^{\text{clip}} = \bar{Z} / \max\{\bar{A}, a/2\}$. Then, for every $B \geq 1$,

$$\mathbb{P}\left(|\bar{A} - a| \geq a/2\right) \leq 2 \exp\left[-\frac{Ba(p)}{12}\right]. \quad (75)$$

Moreover,

$$\mathbb{E}[\hat{\mu}_{\text{SV}}^{\text{clip}}] = \mu_{\text{SV}}(p) + \frac{c_{\text{SV}}(p)}{B} + r_{\text{SV}}^{(E)}(p, B), \quad (76)$$

$$\text{Var}(\hat{\mu}_{\text{SV}}^{\text{clip}}) = \frac{v_{\text{SV}}(p)}{B} + r_{\text{SV}}^{(V)}(p, B), \quad (77)$$

where

$$c_{\text{SV}}(p) = \frac{\mu_{\text{SV}}(p) \text{Var}(A) - \text{Cov}(Z, A)}{a(p)^2} = 0, \quad (78)$$

$$v_{\text{SV}}(p) = \frac{\text{Var}(Z - \mu_{\text{SV}}(p)A)}{a(p)^2}. \quad (79)$$

The equality $c_{\text{SV}}(p) = 0$ is exact, because $Z = AW$ and hence $\text{Cov}(Z, A) = \mathbb{E}[ZA] - \mathbb{E}Z\mathbb{E}A = a\mu_{\text{SV}}(1 - a) = \mu_{\text{SV}} \text{Var}(A)$. There are explicit bounded-moment constants $A_{E,\text{SV}}(p)$, $A_{V,\text{SV}}(p)$ obtained from [Definition 2](#) by the replacement

$$(N_M, D_M, X_M, Y_M, K_{N,M}, K_{D,M}) \mapsto (a\mu_{\text{SV}}, a, Z, A, K_W, 1). \quad (80)$$

With this conservative substitution, put

$$\omega_{\text{SV}}(p) = \frac{1}{a(p)}, \quad (81)$$

$$B_{E,\text{SV}}(p) = \frac{2K_W}{a(p)} \left(5 + 3\omega_{\text{SV}}(p) + 3\omega_{\text{SV}}(p)^2 + 3\omega_{\text{SV}}(p)^3\right), \quad (82)$$

$$B_{V,\text{SV}}(p) = 2B_{E,\text{SV}}(p)^2. \quad (83)$$

Thus

$$\left|r_{\text{SV}}^{(E)}(p, B)\right| \leq \frac{A_{E,\text{SV}}(p)}{B^2} + B_{E,\text{SV}}(p)e^{-Ba(p)/12}, \quad (84)$$

$$\left|r_{\text{SV}}^{(V)}(p, B)\right| \leq \frac{A_{V,\text{SV}}(p)}{B^2} + B_{V,\text{SV}}(p)e^{-Ba(p)/12}. \quad (85)$$

Consequently

$$\text{MSE}_{\text{SV}}(p, B) = b_{\text{SV}}(p)^2 + \frac{v_{\text{SV}}(p)}{B} + \rho_{\text{SV}}(p, B), \quad (86)$$

with $|\rho_{\text{SV}}(p, B)| \leq C_{\text{SV}}(p)B^{-2} + C'_{\text{SV}}(p)e^{-Ba(p)/12}$. One admissible explicit choice is

$$C_{\text{SV}} = A_{V,\text{SV}} + 2|b_{\text{SV}}|A_{E,\text{SV}} + 2A_{E,\text{SV}}^2, \quad (87)$$

$$C'_{\text{SV}} = B_{V,\text{SV}} + 2|b_{\text{SV}}|B_{E,\text{SV}} + 2B_{E,\text{SV}}^2. \quad (88)$$

If $\sigma_{\text{acc}}^2(p) = \text{Var}(W \mid A = 1)$, then

$$v_{\text{SV}}(p) = \frac{\sigma_{\text{acc}}^2(p)}{a(p)}. \quad (89)$$

Therefore, if $\sigma_{\text{acc}}^2(p) = \sigma_{\star}^2 + \sigma_1 p + \mathcal{O}(p^2)$ and $a(p) = 1 - \alpha_{\text{det}} p + \mathcal{O}(p^2)$, then

$$\text{MSE}_{\text{SV}}(p, B) = \delta_{\text{SV}}^2 p^2 + \frac{\sigma_{\star}^2 + (\sigma_1 + \alpha_{\text{det}} \sigma_{\star}^2) p}{B} + \mathcal{O}(p^2/B) + \mathcal{R}_{\text{SV}}(p, B), \quad (90)$$

where no separate $\mathcal{O}(p/B)$ quotient-bias cross term appears: for Bernoulli postselection the coefficient c_{SV} vanishes identically by Equation (78). The certified theorem-level statement is $|\mathcal{R}_{\text{SV}}(p, B)| \leq C_{\text{SV}}(p) B^{-2} + C'_{\text{SV}}(p) e^{-Ba(p)/12}$.

Proof. The acceptance denominator is Bernoulli. The two-sided multiplicative Chernoff bound [32] gives $\mathbb{P}(|\bar{A} - a| \geq \delta a) \leq 2e^{-Ba\delta^2/3}$ for $0 < \delta < 1$; taking $\delta = 1/2$ gives Equation (75). Conditional on the good event $|\bar{A} - a| \leq a/2$, apply the same explicit Neumann expansion used in Theorem 1 to $g(z, a) = z/a$. Because $A \in \{0, 1\}$ and $|Z| \leq K_W$, the moment envelopes are finite and the bad-event contribution is exponentially small. The variance identity follows from

$$Z - \mu_{\text{SV}} A = A(W - \mu_{\text{SV}}), \quad (91)$$

so $\text{Var}(Z - \mu_{\text{SV}} A) = a(p) \sigma_{\text{acc}}^2(p)$. The displayed local expansion follows from Taylor expansion of $1/a(p)$ and from Proposition 4. \square

Remark 7 (Position relative to symmetry expansion). *This SV section is derivative in mechanism from symmetry-based mitigation theory, especially Cai [19]. Cai already compares VD-type symmetry expansion against SV at the level of infidelity and sampling cost. The comparison certified here is different in kind: finite-shot MSE laws with explicit remainders, denominator-concentration certificates, and crossing self-consistency conditions.*

8 PEC and CDR in the selector

The rigorous selector should include only methods whose local constants are specified. PEC can be inserted cleanly under standard first-order cancellation assumptions. Suppose the PEC estimator is unbiased through first order, so

$$b_{\text{PEC}}(p) = \mathcal{O}(p^2), \quad (92)$$

and let $\gamma(p) = 1 + \gamma_1 p + \mathcal{O}(p^2)$ denote the quasiprobability one-norm overhead [2, 34]. Then a local PEC law has the form

$$\text{MSE}_{\text{PEC}}(p, B) = \mathcal{O}(p^4) + \frac{\gamma(p)^2 \sigma_{\text{PEC}}^2(p)}{B} + \mathcal{O}(B^{-2}). \quad (93)$$

Thus PEC fits the selector with $s_{\text{PEC}} \approx \kappa_{\text{PEC}} \gamma^2 \sigma_{\text{PEC}}^2$, where κ_{PEC} accounts for resource normalization.

CDR is different. Its bias and variance depend on the training distribution, regression model, target observable, and allocation of shots between training and target circuits [7, 8]. Therefore CDR should not be included in the rigorous lower envelope unless a separate local law is proven for the chosen training model. Here, CDR remains an admissible future component, not a theorem-level member of the selector.

9 Certified operating-window crossings

Let R be a common physical resource budget. If method m consumes $\kappa_m(p)$ resource units per effective statistical sample, then $B_m = R/\kappa_m(p)$. A certified law becomes

$$\text{MSE}_m(p, R) = b_m(p)^2 + \frac{s_m(p)}{R} + \rho_m(p, R), \quad |\rho_m(p, R)| \leq \frac{C_m(p)}{R^2} \quad (94)$$

for $R \geq R_{\min, m}(p)$, where $s_m = \kappa_m \tilde{v}_m$.

Remark 8 (Resource normalization). *Here R denotes the physical resource being charged in the comparison. If an estimator uses an effective statistical sample count B_m , all streams, copies, and circuit calls required to produce those samples must be included in κ_m . In particular, the independent VD Hadamard-test implementation of [Proposition 2](#) uses one numerator stream and one denominator stream, so a paired VD sample budget B corresponds to physical cost $R_{\text{VD}, M} = 2\kappa_M B$. Equivalently, when R counts physical Hadamard-test calls, $\kappa_{\text{VD}, M} = 2\kappa_M$. Toy-model formulas below state explicitly when R is a paired-shot budget and when it is a physical call budget.*

Theorem 4 (Certified crossing perturbation). *Consider two methods i, j at fixed p . Suppose*

$$\text{MSE}_i = b_i^2 + \frac{s_i}{R} + \rho_i(R), \quad \text{MSE}_j = b_j^2 + \frac{s_j}{R} + \rho_j(R), \quad |\rho_m(R)| \leq \frac{C_m}{R^2} \quad (95)$$

for $R \geq R_{\min}$, and suppose the remainders are continuous. Let

$$g = b_j^2 - b_i^2 > 0, \quad \Delta s = s_i - s_j > 0, \quad R_0 = \frac{\Delta s}{g}, \quad C = C_i + C_j. \quad (96)$$

If $R_0(1 - \eta) \geq R_{\min}$ and

$$\eta = \frac{4C}{gR_0^2} < \frac{1}{2}, \quad (97)$$

then there exists at least one true crossing R^* in

$$R^* \in [R_0(1 - \eta), R_0(1 + \eta)]. \quad (98)$$

In particular every certified crossing in this interval obeys

$$|R^* - R_0| \leq \frac{4C}{gR_0}. \quad (99)$$

If, in addition, $\rho_i - \rho_j$ is differentiable and

$$\sup_{R \in [R_0(1 - \eta), R_0(1 + \eta)]} |(\rho_i - \rho_j)'(R)| < \frac{\Delta s}{R_0^2(1 + \eta)^2}, \quad (100)$$

then the crossing in the interval is unique.

Proof. The leading difference is

$$F_0(R) = (b_i^2 - b_j^2) + \frac{s_i - s_j}{R} = -g + \frac{\Delta s}{R}, \quad (101)$$

with root R_0 . At $R_+ = R_0(1 + \eta)$,

$$F_0(R_+) = -g \frac{\eta}{1 + \eta}, \quad (102)$$

and at $R_- = R_0(1 - \eta)$,

$$F_0(R_-) = g \frac{\eta}{1 - \eta}. \quad (103)$$

The remainder difference has magnitude at most C/R^2 . Since $\eta = 4C/(gR_0^2)$ and $\eta < 1/2$, the signs at R_+ and R_- are preserved. Continuity then gives existence by the intermediate value theorem. If Equation (100) holds, then

$$F'(R) = -\frac{\Delta s}{R^2} + (\rho_i - \rho_j)'(R) < 0 \quad (104)$$

throughout the interval, so the crossing there is unique. \square

The leading indifference formula

$$R_{i \leftrightarrow j}(p) = \frac{s_i(p) - s_j(p)}{b_j(p)^2 - b_i(p)^2} \quad (105)$$

is therefore not accepted automatically. It must pass two checks: $R_{i \leftrightarrow j} \geq R_{\min}$ and $4C/[gR_{i \leftrightarrow j}^2] \ll 1$. This is the self-consistency condition missing from a purely formal crossing curve.

Theorem 5 (Certified selection trichotomy at fixed p). *At fixed p , suppose two methods i, j admit certified local laws*

$$\text{MSE}_m(R) = b_m^2 + \frac{s_m}{R} + \rho_m(R), \quad |\rho_m(R)| \leq \frac{C_m}{R^2}, \quad R \geq R_{\min}, \quad (106)$$

with continuous remainders. Let

$$g = b_j^2 - b_i^2, \quad \Delta s = s_i - s_j, \quad C = C_i + C_j. \quad (107)$$

Then exactly one of the following leading-order regimes applies, with the indicated certified interpretation.

- (0) **Degenerate leading tie.** *If $g = 0$ and $\Delta s = 0$, the two leading local laws are identical. No leading-order dominance or crossing is certified; the comparison depends on the signed remainders, higher-order coefficients, or a sharper local expansion.*
- (I) **Uniform dominance of i .** *If $g > 0$ and $\Delta s \leq 0$, then method i has strictly smaller leading bias and no larger sampling coefficient, and i wins for all*

$$R > \max \left\{ R_{\min}, \sqrt{\frac{C}{g}} \right\}. \quad (108)$$

If $g = 0$ and $\Delta s < 0$, then i has equal leading bias and strictly smaller sampling coefficient, and i wins for all

$$R > \max \left\{ R_{\min}, \frac{C}{|\Delta s|} \right\}. \quad (109)$$

At equality in either displayed threshold, the certificate gives weak non-inferiority rather than strict dominance.

- (II) **Uniform dominance of j .** *If $g < 0$ and $\Delta s \geq 0$, or if $g = 0$ and $\Delta s > 0$, the symmetric statement holds after swapping i and j .*

(III) *Genuine tradeoff with a certified crossing.* If $g\Delta s > 0$, set

$$R_0 = \frac{\Delta s}{g} > 0, \quad \eta = \frac{4C}{|g|R_0^2}. \quad (110)$$

If $\eta < 1/2$ and $R_0(1 - \eta) \geq R_{\min}$, then at least one true crossing lies in

$$[R_0(1 - \eta), R_0(1 + \eta)]. \quad (111)$$

If the monotonicity condition [Equation \(100\)](#) also holds, that crossing is unique in the certified interval. The lower-bias method wins above the certified upper endpoint, and the lower-sampling method wins on the certified neighborhood below the crossing controlled by the same remainder bound; no claim is made for arbitrarily small R , where the C/R^2 term can dominate.

Proof. Write

$$\Phi(R) = \text{MSE}_i(R) - \text{MSE}_j(R) = -g + \frac{\Delta s}{R} + \rho_i(R) - \rho_j(R), \quad |\rho_i(R) - \rho_j(R)| \leq \frac{C}{R^2}. \quad (112)$$

Case (0) is immediate from $g = \Delta s = 0$. Cases (I) and (II) follow because the leading comparison has the same sign for all large enough R , and the C/R^2 remainder cannot overturn it once R exceeds the displayed threshold. In case (III), the leading root is $R_0 = \Delta s/g$. After relabelling if needed so that $g > 0$ and $\Delta s > 0$, the hypotheses reduce exactly to [Theorem 4](#). That theorem gives existence in the certified interval and uniqueness under [Equation \(100\)](#). \square

Corollary 1 (Local location of operating windows). *Suppose*

$$b_m(p) = \delta_m p + \mathcal{O}(p^2), \quad s_m(p) = \sigma_m^2 + s_m^{(1)} p + \mathcal{O}(p^2). \quad (113)$$

Assume $\delta_i^2 \neq \delta_j^2$, so that $b_j(p)^2 - b_i(p)^2 = \Theta(p^2)$. If $\sigma_i^2 \neq \sigma_j^2$, a genuine bias-variance tradeoff has a leading window at scale $R_0 = \Theta(p^{-2})$. If $\sigma_i^2 = \sigma_j^2$ but $s_i^{(1)} \neq s_j^{(1)}$, the leading window is instead at scale $R_0 = \Theta(p^{-1})$. Thus the $1/p$ crossings in the closed toy models below are not accidental; they arise because the two compared laws have matched leading shot cost and differ first at order p in their sampling coefficients.

Proof. Substitute the displayed expansions into $g = b_j^2 - b_i^2$ and $\Delta s = s_i - s_j$. If the constant term of Δs is nonzero, then $R_0 = \Delta s/g = \Theta(p^{-2})$. If that constant term cancels, then $\Delta s = \Theta(p)$ while $g = \Theta(p^2)$, giving $R_0 = \Theta(p^{-1})$. \square

Corollary 2 (Uniform finite-interval sandwich). *Suppose on $p \in [0, p_{\max}]$ one has computable bounds*

$$0 < G_-(p) \leq b_j(p)^2 - b_i(p)^2 \leq G_+(p), \quad 0 < S_-(p) \leq s_i(p) - s_j(p) \leq S_+(p). \quad (114)$$

Then the leading crossing satisfies

$$\frac{S_-(p)}{G_+(p)} \leq R_{i \leftrightarrow j}(p) \leq \frac{S_+(p)}{G_-(p)}. \quad (115)$$

If the certified-remainder condition of [Theorem 4](#) holds uniformly on that interval, this becomes a two-sided finite- p operating-window certificate, not merely a Taylor expansion at $p = 0$.

10 Restricted lower-bound sanity check

The selector constructed above compares concrete mitigation procedures. It does not by itself prove that the selected method is globally optimal among all conceivable estimators. A full optimality theorem would require specifying what information about the noise channel, ideal state family, measurements, and adaptive strategies is available. Universal sampling-cost lower bounds for error mitigation, typically exponential in circuit noise, have been established [35–38]. The bound here is narrower and complementary: it benchmarks a declared transcript model at fixed budget, rather than bounding all mitigation strategies. It identifies when an operating window is limited by statistical distinguishability rather than by the chosen menu of methods.

Consider a local two-point model indexed by $\theta \in \{+, -\}$. The ideal values are

$$\mu_\theta^* = \text{Tr}(O\rho_\theta^*), \quad |\mu_+^* - \mu_-^*| = 2h. \quad (116)$$

At physical noise level p , a resource budget R , and a fixed admissible measurement and mitigation protocol induce transcript distributions $\mathbb{P}_+^{(R)}$ and $\mathbb{P}_-^{(R)}$. These transcript distributions include all random circuits, accepted or rejected shots, auxiliary calibration samples, and classical postprocessing randomness used by the protocol.

Theorem 6 (Two-point finite-budget lower bound). *For any estimator $\hat{\mu}$ of the ideal value based on the transcript,*

$$\sup_{\theta \in \{+, -\}} \mathbb{E}_\theta [(\hat{\mu} - \mu_\theta^*)^2] \geq \frac{h^2}{2} \left(1 - \text{TV}(\mathbb{P}_+^{(R)}, \mathbb{P}_-^{(R)})\right), \quad (117)$$

where TV denotes total variation distance. Consequently, if

$$\text{KL}(\mathbb{P}_+^{(R)} \parallel \mathbb{P}_-^{(R)}) \leq RI_p h^2, \quad (118)$$

then

$$\sup_\theta \mathbb{E}_\theta [(\hat{\mu} - \mu_\theta^*)^2] \geq \frac{h^2}{2} \left(1 - \sqrt{\frac{RI_p h^2}{2}}\right)_+. \quad (119)$$

Choosing $h = (2RI_p)^{-1/2}$, whenever this perturbation lies inside the local model, gives the sampling lower bound

$$\sup_\theta \mathbb{E}_\theta [(\hat{\mu} - \mu_\theta^*)^2] \geq \frac{1}{8RI_p}. \quad (120)$$

Proof. Threshold $\hat{\mu}$ at the midpoint between μ_-^* and μ_+^* . Under hypothesis θ , this test can err only if $|\hat{\mu} - \mu_\theta^*| \geq h$, so Markov’s inequality gives

$$\mathbb{P}_\theta(\text{err}) \leq \frac{\mathbb{E}_\theta[(\hat{\mu} - \mu_\theta^*)^2]}{h^2}. \quad (121)$$

Le Cam’s two-point testing argument [39, 40] gives that the minimum possible sum of the two testing errors is $1 - \text{TV}(\mathbb{P}_+^{(R)}, \mathbb{P}_-^{(R)})$. Taking the larger of the two risks to be at least their average gives Equation (117). Pinsker’s inequality gives

$$\text{TV}(\mathbb{P}_+^{(R)}, \mathbb{P}_-^{(R)}) \leq \sqrt{\frac{1}{2} \text{KL}(\mathbb{P}_+^{(R)} \parallel \mathbb{P}_-^{(R)})}, \quad (122)$$

which yields Equation (119). The choice of h gives Equation (120). \square

Corollary 3 (Structural non-identifiability floor). *If two distinct ideal values satisfy $|\mu_+^* - \mu_-^*| = 2h$ but induce the same noisy transcript distribution for every budget R , then every estimator obeys*

$$\sup_{\theta \in \{+, -\}} \mathbb{E}_\theta \left[(\hat{\mu} - \mu_\theta^*)^2 \right] \geq \frac{h^2}{2}. \quad (123)$$

Thus a budget-independent floor is unavoidable whenever the ideal functional is not identifiable from the noisy experiment and side information allowed to the protocol.

Remark 9 (How this lower bound should be used). *This is not a universal no-go theorem for QEM. It is a restricted benchmark for a declared statistical model. Its value is diagnostic. If a VD/SV/PEC operating window lies far above Equation (120), the method menu or constants may be improvable. If it approaches the two-point lower bound inside the same model, the selector is close to statistically optimal in that restricted sense. The corollary also clarifies why bias floors matter: some floors are not artifacts of a mitigation method but consequences of information that the noisy transcript does not contain.*

Explicit constants instantiating this bound for a one-qubit Bernoulli transcript ($I_p^{\text{Bern}} = 4(1-p)^2$, giving the concrete floor $1/[32R(1-p)^2]$), together with an accepted-transcript Fisher-efficiency statement for the SV estimator, are developed in Propositions D.1 and D.2; the selector toy model saturates them up to the stated conservative factors.

11 Toy models with closed constants

Three fully explicit toy models instantiate every constant in the framework and are developed in Section D. First, a one-qubit Bernoulli selector toy admits closed-form quotient constants and a certified finite- p sandwich, and saturates the restricted two-point lower bound up to the explicit factors of Section 10 (Proposition D.5). Second, a fixed-sector toy with $\delta_{\text{SV}} \neq 0$ yields an operational Efron–Stein certificate with numerical constants (Proposition D.7) and an explicit VD-versus-SV crossing (Proposition D.6). Third, a generic heterogeneous-noise toy exhibits simultaneously nonvanishing δ_{VD} and δ_{SV} , the case probed by the Level 1 experiments E3–E4.

12 Experimental validation

The numerical evidence is organized as a three-level hierarchy. The hierarchy matters: coefficient-level claims are tested only in Level 1, where the simulator is an exact white-box density-matrix model and the closed-form quantities can be compared directly against ground truth. Level 2 and Level 3 test form, robustness, and operational feasibility under more realistic circuit assumptions; they are not used to validate the constants δ_{VD} , δ_{SV} , c_{VD} , c_{SV} , or the certified remainder coefficients.

12.1 Level 1: white-box coefficient checks

Level 1 is the main reproducible numerical layer. It uses fixed QAOA instances in a fixed Hamming-weight sector [42, 43] and compares the fitted finite-shot laws with exact density-matrix quantities. In this experimental subsection, $\hat{\beta}_0^{\text{fit}}, \hat{\beta}_1^{\text{fit}}, \hat{\beta}_2^{\text{fit}}$ denote WLS coefficients in the empirical regression of MSE against $1/B$; in particular, $\hat{\beta}_0^{\text{fit}}$ estimates b^2 and $\hat{\beta}_1^{\text{fit}}$ estimates the leading MSE coefficient $\tilde{v} = v + 2bc$. These fit coefficients are distinct from the local unmitigated-bias coefficient $\beta_0 = \text{Tr}(O\Delta)$ in Equation (9). The pre-specified

Layer	Model	Claim supported
Level 1	Exact white-box density-matrix QAOA instances	Coefficient and structural checks against closed-form ground truth.
Level 2	Seeded Qiskit/Aer gate-level simulation with synthetic thermal and readout noise	Form and robustness of the operating-window laws under realistic state-preparation and VD-interferometry overhead.
Level 3	Archived IBM <code>ibm_marrakesh</code> hardware counts with calibrated readout	Qualitative feasibility and inter-instance robustness on hardware; no coefficient-level inference.

Table 1: Experimental claim hierarchy.

primary validation criteria [44] were deliberately strict: under the amended v2 run, P1 did not satisfy the all-instance validation rule. This is a strict validation outcome, not evidence against the quotient law. The VD curvature signal was present in every instance, with $\Delta\text{AIC} > 2$ [45, 46] in 10/10 and the fitted curvature $\hat{\beta}_2^{\text{fit}}$ excluding zero in 10/10. The closed-form leading MSE coefficient \tilde{v} was covered by the $\hat{\beta}_1^{\text{fit}}$ interval in 8/10 v2 instances rather than 10/10, while the same closed form was covered in 10/10 in the v1 run. The two v2 $\hat{\beta}_1^{\text{fit}}$ misses, `g6_k2_c000` and `g6_k2_c002`, have standardized deviations $z = 2.30$ and $z = 2.01$, respectively, which are within the calibration-noise band.

The post-run ensemble calibration gives the corresponding context. If each interval has nominal 95% coverage and the coefficient is correct, a 10/10 conjunction succeeds with probability only $0.95^{10} \simeq 0.60$; observing 8/10 covered intervals has binomial lower-tail probability about 0.086. The pooled residual statistic for v2 $\hat{\beta}_1^{\text{fit}}$ is also consistent with nominal ensemble coverage, with $\chi^2 p \simeq 0.16$ and mean $z = -0.575$. Moreover, P1 contains multiple all-instance interval checks: even just two independent 95%-coverage 10/10 checks would pass with probability about $(0.95^{10})^2 \simeq 0.36$. The calibration therefore treats Level 1 as strong structural and diagnostic evidence, while preserving the archive record that the primary all-instance rule was over-strict for this validation family.

The secondary theorem-validation family in Table 3 is separate from the primary validation family. It is still Level 1 white-box evidence against closed-form ground truth, not coefficient validation on a device. The family validates the leading-window location and selection-trichotomy patterns at $C = 0$, including 300/300 sign matches and $R^2 \simeq 0.9999$ for the p^{-2} VD2-versus-unmitigated scaling, but it does not test the formal certified remainders. It also checks the multiplicative implementation-noise baseline, the Le Cam constants 64/32 in the toy where the bound is derived, with Fisher saturation $sJ = 1$, and the Efron–Stein operational certificate in 60/60 sampled cells. The Efron–Stein constants are on an operational 10^3 scale rather than the formal 10^8 reference scale, while the E6 copy-log check is reported only mechanistically because $M^*(B)$ itself is not resolvable in the fixed configuration.

The pre-specified resource-normalization and observable-convention sensitivity check (E7) completes the Level 1 family. Across the eight pre-specified convention combinations—four resource definitions (paired sample, Hadamard call, two-qubit-gate proxy, wall-clock proxy) and two observable normalizations—no pairwise comparison changes its large-resource winner in any of the ten fixed instances: VD-versus-unmitigated retains a genuine leading crossing in 80/80 cells, and the VD-versus-SV classification is identical under every convention. The only convention-dependent feature is whether SV-versus-unmitigated

Check	Status	Main result
P1/E1 VD quotient law	All-instance criterion not met	VD $\Delta\text{AIC} > 2$ in 10/10; VD curvature $\widehat{\beta}_2^{\text{fit}}$ excludes zero in 10/10; closed-form \tilde{v} covered by $\widehat{\beta}_1^{\text{fit}}$ in 8/10 in v2 and 10/10 in v1.
P2/E1 intercept	Descriptive after primary criterion	Closed-form b^2 covered by $\widehat{\beta}_0^{\text{fit}}$ in 9/10.
P3–P4/E2 c_{VD} vs c_{SV}	Descriptive after primary criterion	c_{VD} passes 30/30 instance- p cells; c_{SV} is within the fixed TOST margin [47] in 29/30.
P5–P6/E3–E4 first-order slopes	Descriptive after primary criterion	Non-near-zero δ_{VD} cases pass 7/7; non-near-zero δ_{SV} cases pass 9/9.
P7/E5 denominator concentration	Secondary check met	Median bad-denominator probability drops from about 0.091 at $0.125B_{\text{den}}$ to 9×10^{-5} at B_{den} and effectively zero at $2B_{\text{den}}$.
P9/E7 crossing band	Secondary check mixed	The operational self-consistency parameter satisfies $\eta < 1/2$ in 10/10, but the fitted crossing lies in the operational band in 6/10.

Table 2: Level 1 validation summary. The table translates the archived status label into plain language, while the ensemble calibration shows that the missed all-instance criterion is consistent with nominal coverage rather than evidence against the quotient law. The B_{den} scale in the P7 row is the one-sided threshold of Remark 3 at $\varepsilon = 10^{-3}$.

appears as uniform SV dominance or as a finite crossing: the wall-clock proxy, which charges SV a small postselection bookkeeping cost, converts 6 of 20 instance-normalization cells from dominance to a crossing without changing the large-resource winner. Crossing conclusions therefore do not flip under the declared resource or observable conventions.

The two remaining pre-specified robustness checks close the same way. Replacing the clipping floor $D_M/2$ by $D_M/3$ or $2D_M/3$ leaves the fitted leading coefficient unchanged on the fixed ensemble: with common random numbers the three clipped estimators coincide on every draw without a clip event, the clip rate is zero at the largest budgets, and the fitted $\widehat{\beta}_1^{\text{fit}}$ values agree within 2.4% relative deviation across all instances and thresholds. Under a heterogeneous depolarizing channel, the white-box first-order slopes follow the closed-form generators in 10/10 instances, with maximum absolute error 5×10^{-11} for δ_{VD} ; δ_{SV} vanishes to machine precision, exactly as Remark 6 predicts, while δ_{VD} remains generic.

This distinction is important for interpretation. A genuine coefficient mismatch in Level 1 would be evidence of a theory, implementation, or estimator error. The observed pattern is different: the VD curvature, $c_{\text{VD}} \neq 0$ versus $c_{\text{SV}} \approx 0$ distinction, first-order generator slopes, and denominator scale all appear with the expected structure. Figure 1 shows the ensemble-coverage diagnosis behind the 8/10 P1 outcome. The limitation is the calibration of the all-instances validation rule, not the closed-form coefficient.

Figures 2 and 3 display the coefficient-level diagnostics associated with P1–P6, while Figures 4 and 5 display the denominator and crossing diagnostics associated with P7 and P9.

12.2 Level 2: device-simulation operating windows

Level 2 asks whether the finite-shot operating-window laws survive in form under a gate-level Qiskit/Aer model [26]. The model uses Trotterized QAOA state preparation with a synthetic thermal-plus-readout noise model. The reference value is the noiseless Level 2 circuit, not the exact Level 1 dense-mixer state. Thus Level 2 is a device-form validation

Experiment	Paper result	Check	Secondary outcome
E6/P8	Theorem 2	Copy-log scale mechanism	The pre-specified $M^*(B)$ regression is not resolvable because the floor is reached in only a few copies. The mechanism checks pass: $b_M - b_\infty \sim q^M$ has slope -5.23 versus -5.04 , and $\tilde{v}_M \sim \lambda_1^{-2M}$ has slope 0.1033 versus 0.1032 .
E8	Corollary 1	Window location, leading law $C = 0$	VD2-versus-unmitigated recovers the p^{-2} scale in 10/10 instances, with mean exponent -1.966 and mean $R^2 \simeq 0.9999$. SV-versus-unmitigated has no valid positive crossing in 0/10: the leading variances match at $p = 0$ and the order- p split also favors SV, giving uniform dominance.
E9	Theorem 5	Selection trichotomy, leading law $C = 0$	Predicted and observed signs match in 300/300 cells. VD-versus-unmitigated gives 100/100 crossings; SV-versus-unmitigated gives 99/100 dominance cells; VD-versus-SV gives 73 dominance cells and 27 crossings.
E10	Proposition 3	Implementation-noise baseline	Common-contraction bias invariance passes 10/10, the variance formula passes 10/10 at tolerance 0.02, and the asymmetric-bias shift passes 10/10 at 4 SE. Mean variance inflation is 1.24 for $\eta = 0.9$ and 1.57 for $\eta = 0.8$.
E11	Proposition D.5	Le Cam constants in the deriving toy	This is an arithmetic consistency check, not independent QAOA evidence. MSE divided by the conservative bound is ≤ 64 in 72/72, MSE divided by the local bound is ≤ 32 in 72/72, and $sJ = 1$ to 10^{-12} in 72/72.
E12	Lemma 3 and Proposition D.7	Efron–Stein operational certificate	The sampled certificate $\text{Var}_{\text{emp}} \leq ES/B$ holds in 60/60 cells. The median ES constant is about 1.03×10^3 , compared with the formal 10^8 scale reference; under the ES law, SV dominates VD in 5/10 instances.

Table 3: Secondary Level 1 theorem-validation family. These checks are descriptive white-box comparisons against closed-form quantities and do not enter the primary family of pre-specified validation checks.

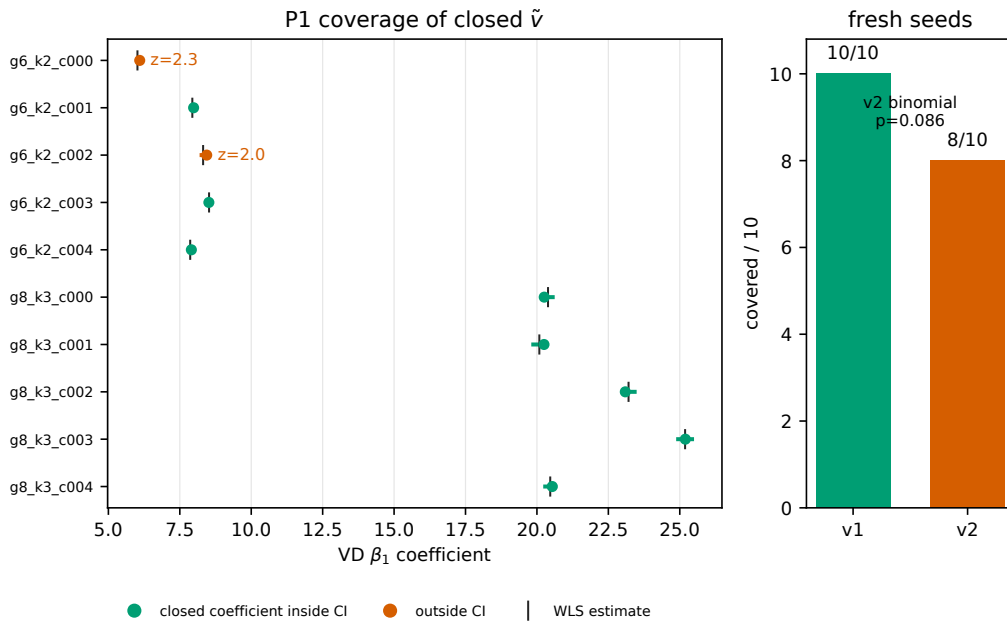


Figure 1: Level 1 coverage audit for the P1 leading VD MSE coefficient. The horizontal intervals are WLS 95% intervals for β_1^{fit} , the dots are the closed-form \tilde{v} , and orange marks the two v2 instances outside the interval. The same coefficient covered 10/10 instances in v1 and 8/10 in v2; the v2 outcome has binomial lower-tail probability 0.086 under nominal 95% coverage.

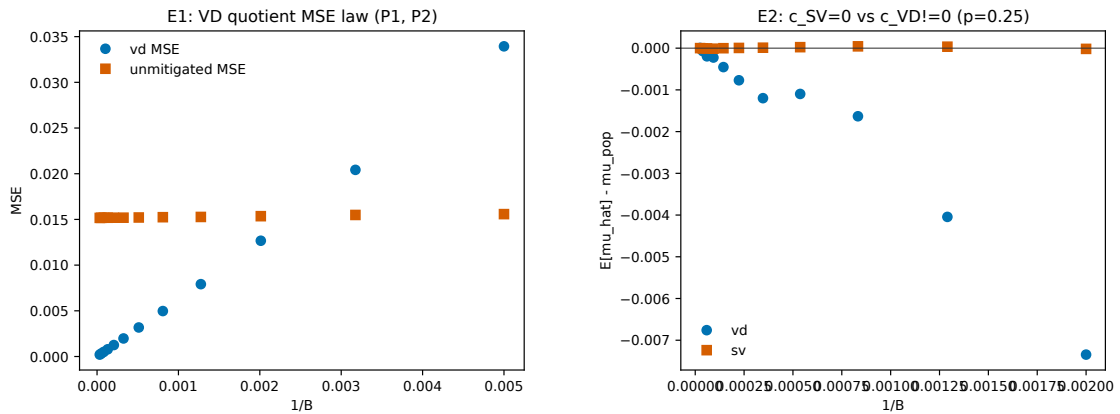


Figure 2: Level 1 quotient-law and c -coefficient diagnostics from the amended v2 run. Left: E1 MSE versus $1/B$ for the primary instance used in the figure, illustrating the VD quotient curvature. Right: E2 separates the nonzero VD quotient-bias slope from the SV slope centered near zero.

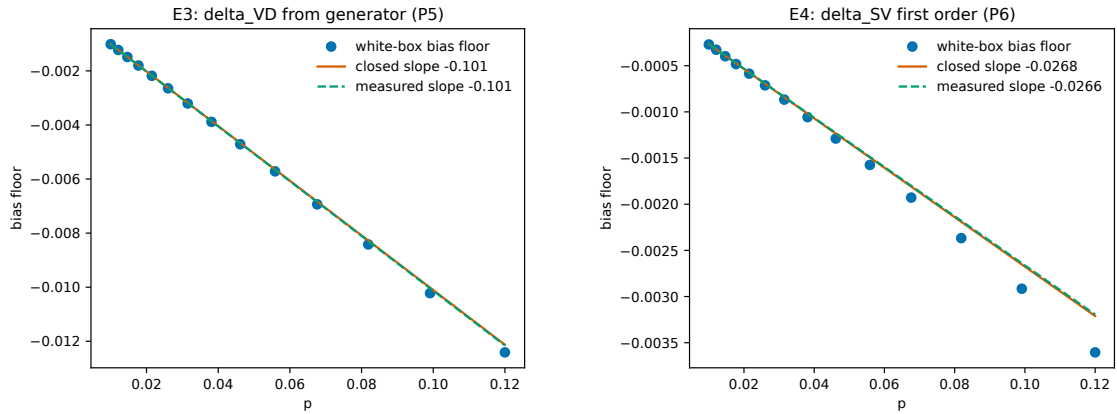


Figure 3: Level 1 first-order bias-floor checks from the amended v2 run. The measured white-box slopes track the generator formulas for δ_{VD} and δ_{SV} on the primary plotted instance.

layer, not a coefficient-validation layer. The pre-specified Level 2 validation metrics P10 and P13 are the device-level counterparts of the white-box checks E8 (window-location scaling) and E12 (Efron–Stein certificate), respectively.

In the high-power exact- ρ harness, the observed finite-shot structure is clear: method-dependent population-bias floors plus sampling contributions that decrease with B . Pooled over the $n = 6$ and $n = 8$ instances, the median absolute empirical bias is about 0.104 for the unmitigated estimator, 0.0145 for SV, and 0.0549 for an optimistic state-noise-only $M = 2$ VD contrast. The corresponding pooled median MSE values are 0.0110, 3.65×10^{-4} , and 0.0332. These pooled summaries do not establish a universal ordering: the $n = 6$ and $n = 8$ regimes differ, and the $n = 8$ cases have much smaller D_2 , close to a denominator-concentration stress test.

The optimistic VD rows are best-case contrasts: they omit the cost of implementing the two-copy quotient on a device. A realistic $n = 6$ follow-up includes Hadamard/SWAP interferometry, controlled-SWAP decomposition, gate noise, and readout. In that circuit-level test, realistic VD has 0/5 bias-floor wins over SV, 0/5 large- B MSE wins at paired-sample resource, and 0/5 large- B MSE wins under the two-qubit-gate proxy. The mechanism is visible in the overhead columns: for g6_k2_c000, realistic interferometry raises the VD bias floor by about 2.8 times relative to the optimistic state-noise-only contrast, and the median inflation over the five $n = 6$ instances is about 3.3 times.

The denominator and window diagnostics show the same operating-window mechanism. Exact denominator-tail calculations give a median $\mathbb{P}(\hat{D}_M < D_M/2)$ of about 0.12 at $0.1B_{\text{den}}$, 9.2×10^{-5} at B_{den} , and 1.8×10^{-32} at $10B_{\text{den}}$. Here and throughout, B_{den} is the one-sided threshold of Remark 3. This Level 2 denominator sweep uses a different low- B grid point from the Level 1 P7 summary, $0.1B_{\text{den}}$ rather than $0.125B_{\text{den}}$, but both probe the same threshold scale. The selected VD-versus-SV comparison is SV-dominant or large-resource SV-winning in 10/10 instances under the two-qubit proxy. At the same time, the optimistic $n = 6$ state-noise-only contrast has a VD large-resource window in 2/5 comparisons, showing that VD distillation itself is not intrinsically weak; the realistic interferometry overhead removes that window in this device-simulation regime. Finally, the controlled small-gate-noise variant recovers the P10 scaling in form. The median VD-optimal-versus-unmitigated exponent is -1.95 , close to the predicted -2 . For SV versus unmitigated, only 2/10 instances have positive matched crossings; their exponents are -0.99 and -0.89 , consistent with the predicted -1 , while the other instances are reported

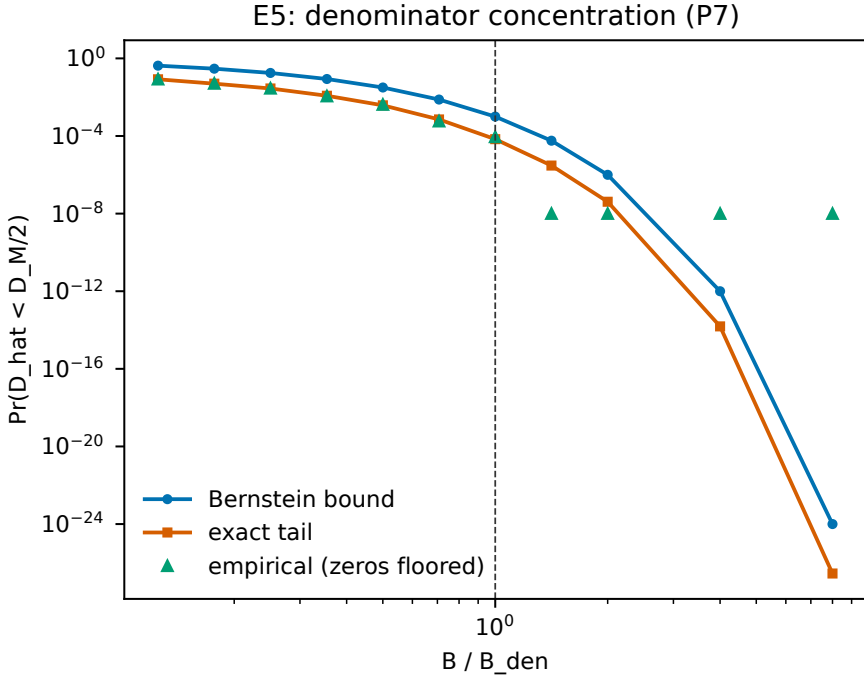


Figure 4: Level 1 denominator-concentration diagnostic from the amended v2 run. The bad-denominator probability collapses around the predicted scale B_{den} , matching the P7 interpretation in Table 2.

as having insufficient positive crossings rather than being forced into the fit.

Table 4 and Figures 6 and 7 summarize the Level 2 evidence without changing its claim level. The device model is synthetic because no `FakeBackendV2` provider was available in the installed Level 2 environment, and the $n = 8$ cases remain an extreme-decoherence stress regime with $D_2 \simeq 0.007$. The folded P10 sweep uses global unitary folding [48] with $\lambda \in \{1, 3, 5, 7\}$, which is a device-depth amplification diagnostic rather than the analytic small- p knob. It does not recover the P10 exponents: readout floors, base noise, and global depth amplification dominate, giving an SV-versus-unmitigated median slope about 0.063 rather than -1 . This is reported as a regime limitation, not as a failure of the theorem; it is why the separate small-gate-noise variant is the appropriate asymptotic P10 check.

The Level 2 Efron–Stein/P13 analysis is the device-simulation counterpart of Lemma 3 and Proposition D.7. It is mathematically meaningful as a variance certificate, but it does not create a practical VD-over-SV operating point in this device-simulation regime. For selected VD, finite two-qubit-proxy R_{ES} rows occur in 0/10 instances and selected VD dominates at R_{ES} in 0/10; even the optimistic contrast reaches only non-operational finite thresholds, with maximum $R_{\text{ES}} \simeq 5.2 \times 10^9$. The ES constants are much larger than in the Level 1 white-box certificate, about 1.6×10^6 – 3.9×10^6 for realistic $n = 6$ selected VD and 4.8×10^{10} – 6.5×10^{10} for the $n = 8$ a-fortiori optimistic rows, so the certificate is not a route to operational VD dominance here.

12.3 Level 3: hardware robustness

Level 3 is an archive-only IBM-hardware robustness layer with a primary `ibm_marrakesh` run and an independent cross-backend replicate on `ibm_kingston`. The analysis uses readout calibration [27, 28] and cluster bootstrap over calibration epochs [49]. It is qualitative hardware evidence: it tests whether the Level 2 operating-window story remains visible on

Prediction	Level 2 result	State	Key evidence
Finite-shot MSE shape	Bias floors plus finite-shot variance are visible	Validated in form	Pooled medians: absolute bias 0.104 for unmitigated and 0.0145 for SV; MSE 0.011 for unmitigated and 3.65×10^{-4} for SV.
P7/E5 denominator concentration	Bad-denominator probability collapses around B_{den}	Validated in form	Median exact $\mathbb{P}(\hat{D} < D/2)$ is about 0.12 at $0.1B_{\text{den}}$, 9.2×10^{-5} at B_{den} , and 1.8×10^{-32} at $10B_{\text{den}}$.
P9/E7 crossings	SV dominates selected realistic/a-fortiori VD across the ensemble	Validated in form, with operating-window caveat	SV is the large-resource winner versus unmitigated in 10/10; selected VD-versus-SV is SV-dominant or large-resource SV-winning in 10/10; the optimistic $n = 6$ VD window appears in 2/5.
P10/E8 folded sweep	Global unitary folding is outside the small-noise asymptotic regime	Limitation reported	Folded SV-versus-unmitigated has median slope 0.063 versus the -1 asymptotic prediction; VD-optimal-versus-SV has insufficient positive crossings.
P10/E8 small-noise variant	Direct small gate-noise scaling recovers P10 in form	Validated in form	VD-optimal-versus-unmitigated has median exponent -1.95 with $R^2 \simeq 0.9999$; SV-versus-unmitigated gives -0.99 and -0.89 only in the 2/10 instances with positive crossings.
P13/E12 Efron–Stein device bound	The ES threshold is not an operational VD-over-SV window	Validated in form as non-operational	Selected VD has finite two-qubit-proxy R_{ES} rows in 0/10 and dominates at R_{ES} in 0/10; the optimistic contrast has maximum finite $R_{\text{ES}} \simeq 5.2 \times 10^9$.

Table 4: Level 2 prediction-to-result map. Level 2 validates operating-window laws in form under the synthetic Aer thermal/readout model documented in the artifact, not Level 1 coefficients. The optimistic VD rows are best-case state-noise-only contrasts; realistic $n = 6$ VD includes Hadamard/SWAP interferometry, controlled-SWAP decomposition, gate noise, and readout.

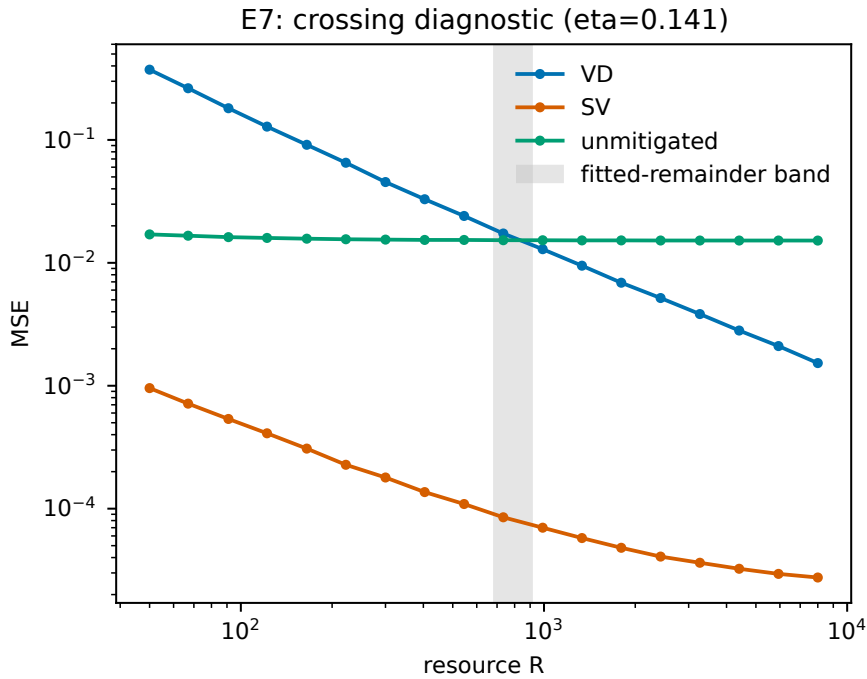


Figure 5: Level 1 crossing diagnostic from the amended v2 run. The shaded region is the fitted-remainder operational band around the leading crossing scale used for P9; this is a diagnostic fitted- C band, not the formal conservative certificate.

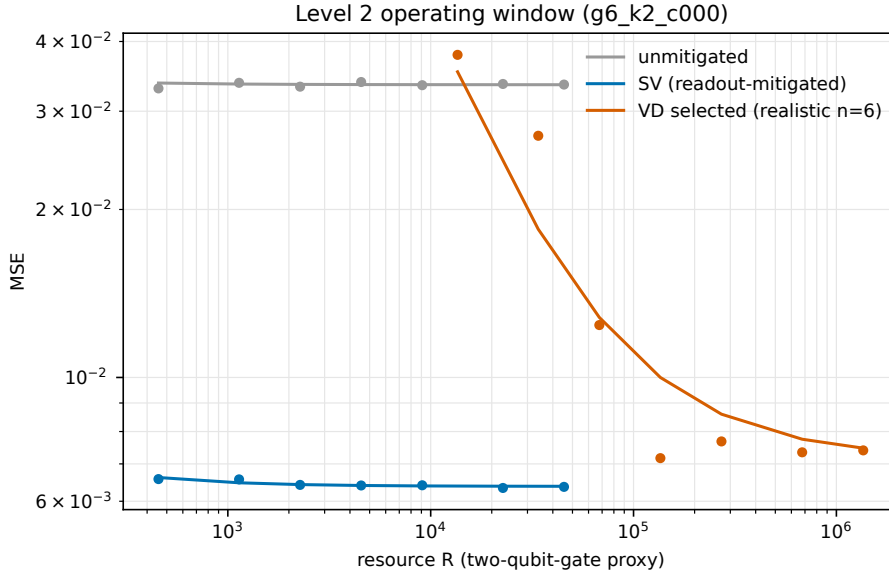


Figure 6: Representative Level 2 operating-window curve for `g6_k2_c000` under the two-qubit-gate proxy. Lines are fitted law curves and points are sampled MSE values from the E7/P9 Level 2 analysis. The selected VD curve is the realistic $n = 6$ interferometry-including device circuit; SV remains below both unmitigated and selected VD on the plotted resource range.

real hardware, but it does not estimate the analytic coefficients.

The primary hardware ordering in [Table 5](#) and [Figure 8](#) is consistent across two $n = 6$

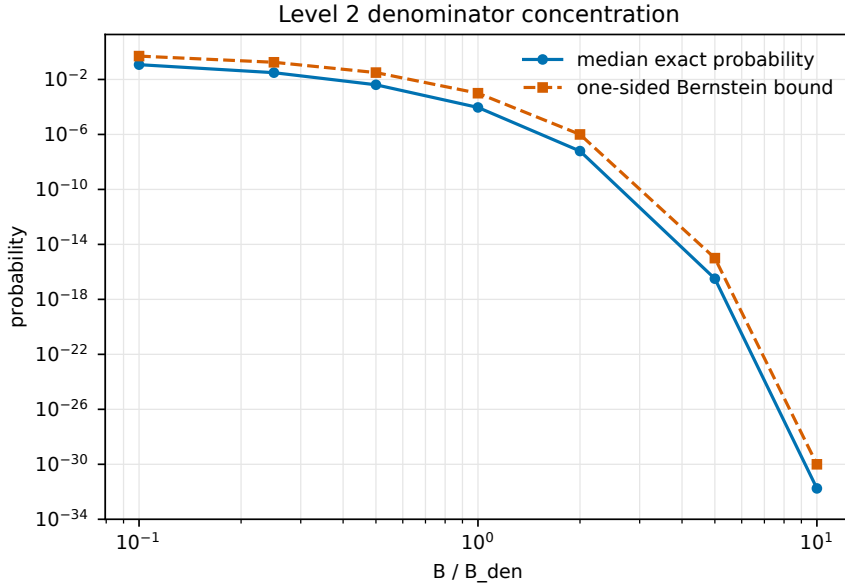


Figure 7: Level 2 denominator concentration in the E5/P7 device-simulation layer. The plot shows the median exact bad-denominator probability and the median one-sided Bernstein bound of Equation (53) versus B/B_{den} , computed from the same Level 2 denominator table used in Table 4.

Instance	n	Epochs	SV MSE	Unmitigated MSE	VD MSE/status
g6_k2_c000	6	38	0.0103	0.0450	0.0741
g6_k2_c001	6	16	5.5×10^{-4}	0.0151	0.0491
g8_k3_c000	8	12	1.5×10^{-4}	0.0219	diverges ($\hat{D} \approx 0$)

Table 5: Largest- B hardware MSE summary at $B = 8192$. Entries are point estimates rounded for readability; the qualitative ordering was assessed using epoch-cluster bootstrap. The raw $n = 8$ VD point estimate is 6.8×10^6 , reported here as denominator blow-up rather than as an ordinary comparable MSE scale.

Backend/analysis	Epochs	SV MSE	Unmit. MSE	VD MSE
ibm_marrakesh primary	38	0.0103	0.0450	0.0741
ibm_kingston fixed replicate	14	0.0103	0.0415	0.0489
ibm_kingston all-19 sensitivity	19	0.0103	0.0414	0.0503

Table 6: Cross-backend Level 3 replicate for g6_k2_c000 at $B = 8192$. Every row has the same order, $\text{SV} < \text{unmitigated} < \text{VD}$. The `ibm_kingston` primary replicate used 14 fixed epochs under a result-blind stop rule. The all-19 sensitivity row includes five later archived jobs that were excluded deterministically from the primary analysis; it is reported only as a result-blind sensitivity check.

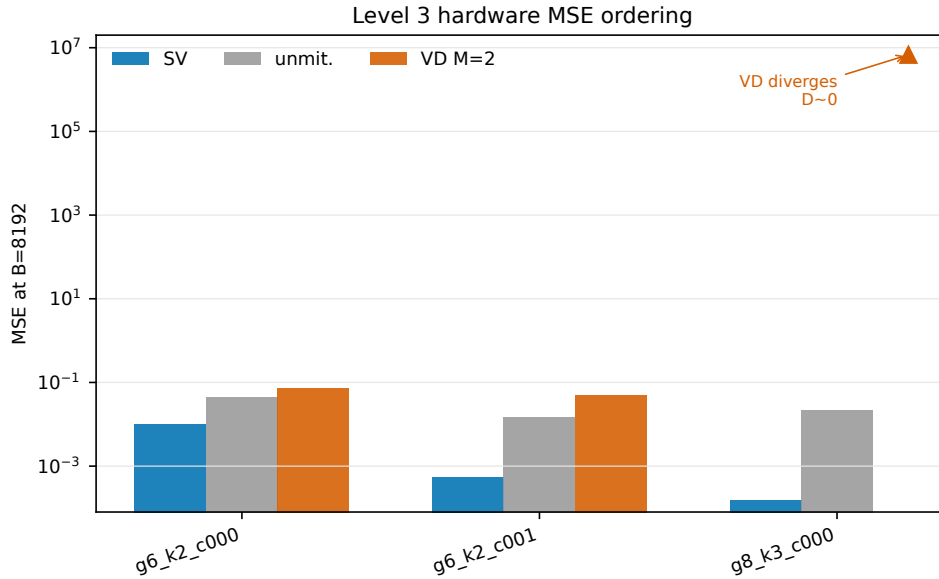


Figure 8: Level 3 hardware MSE at $B = 8192$ from archived `ibm_marrakesh` analyses. The y-axis is logarithmic. The $n = 8$ VD point is annotated as denominator blow-up, not as an ordinary comparable MSE bar.

instances and one $n = 8$ instance on `ibm_marrakesh`. In the $n = 8$ case, the $M = 2$ VD circuit requires a 17-qubit compiled circuit with depth 3192, and the readout-mitigated denominator is extremely small; the quotient blows up while SV remains stable. The independent `ibm_kingston` replicate in Table 6 repeats the same $B = 8192$ ordering for `g6_k2_c000`, namely $SV < \text{unmitigated} < VD$. The all-19 Kingston sensitivity analysis, which includes five archived jobs excluded from the fixed 14-epoch primary replicate by a deterministic result-blind rule, leaves the ordering unchanged. Thus the Level 3 ordering is not confined to a Marrakesh-only calibration snapshot, although it remains a qualitative one-instance cross-backend robustness check rather than hardware coefficient validation.

The hardware P7/P9 behavior has the same form as the denominator and crossing diagnostics in Lemma 2 and Theorem 4, but only qualitatively. For `g6_k2_c000`, the readout-mitigated VD denominator is small, with $B/B_{\text{den}} \simeq 0.62$ at $B = 8192$ on `ibm_marrakesh` and $B/B_{\text{den}} \simeq 1.9$ on the fixed `ibm_kingston` replicate. The Marrakesh point remains below the denominator-concentration scale, while Kingston exceeds it at the largest B but VD still loses because of quotient bias and epoch-level variance. No VD-over-SV crossing is resolved on the available hardware B -grid and budget. Level 3 therefore supports the same qualitative conclusion as Level 2: calibrated SV has lower MSE in the tested QAOA hardware instances, whereas realistic VD overhead and denominator instability move the optimistic VD window outside the available hardware grid and budget.

12.4 Synthesis

The combined validation picture matches the mathematical thesis without overstating the evidence. There is no regime-independent winner. VD is favored in deliberately VD-friendly toy regimes and can show an ideal state-noise-only window in moderate-noise $n = 6$ cases. In the tested realistic QAOA simulations and archived hardware runs, however, SV has lower MSE after sector postselection and readout calibration because the VD quotient pays both denominator-concentration and interferometry-overhead costs. Level 1 supports

the coefficient formulas structurally while noting that the pre-specified all-instance criterion was not met; Levels 2–3 support the operating-window form and practical ordering, not analytic coefficient validation. The device-level lesson is therefore regime-dependent: an ideal VD advantage does not imply an operational one. The operating-window certificates identify where the gap comes from—quotient instability and implementation overhead—rather than leaving the hardware ordering as an unexplained benchmark reversal.

13 Reproducibility and data availability

The accompanying artifact is organized so that the level of reproducibility matches the level of claim. The Level 1 coefficient-checking layer is the main reproducible core: it uses a white-box density-matrix implementation, fixed instances and thresholds, and reference outputs checked by a verifier. The fixed analysis plan has two archived hashes, and the amended v2 package passes a zero-drift check. A reviewer can rerun the Level 1 reference verification without Qiskit or any quantum-cloud account.

Level 2 is a seeded Qiskit/Aer device-simulation layer. Its outputs are included as a form-validation and robustness layer, but they are not mixed into the tight Level 1 reference tier. They are documented as generated artifacts with seeds and reports, outside the Level 1 reference tier.

Level 3 is hardware analysis-reproducible only. The raw IBM count archives, job identifiers, backend provenance, transpilation summaries, layouts, and calibration-epoch metadata are archived. Public reproduction reruns only the analysis from those archives; it does not require, and should not attempt, new QPU submissions. Hardware credentials are not stored in the repository.

The release package includes the code repository, archived analysis-plan hashes, reference outputs, archived hardware counts, exact dependency lockfiles, and release metadata. The repository is public at <https://github.com/vicenzoscavino1999/finite-shot-vd-sv>, and the exact release used for this manuscript (v1.0.1) is archived at Zenodo under DOI [10.5281/zenodo.20682998](https://doi.org/10.5281/zenodo.20682998).

14 Scope and limitations

We prove conditional local laws, explicit quotient certificates, implementation-level VD variance constants for an idealized Hadamard/derangement estimator, a sharper Efron–Stein total-variance diagnostic, an asymptotic second-order quotient-variance diagnostic, finite-interval toy boundaries, a multiplicative implementation-noise baseline, and a restricted Le Cam lower bound. The general toy certificates are numerically conservative; their large constants certify non-vacuity but are not intended as tight physical thresholds. In the first closed toy, however, the direct SV second-order quotient calculation gives an operational remainder of order one and certifies the crossing at ordinary small-noise parameters. The validation layer instantiates concrete QAOA instances, a concrete SV projector, realistic VD interferometry circuits, Aer device simulation, and qualitative IBM-hardware checks. Those additions test form and feasibility, but they do not prove a global optimality theorem over all possible QEM protocols. Such a theorem would require a fully specified statistical decision model for estimating an ideal functional μ_\star from noisy states ρ_p , including what is known about the noise channel and which adaptive measurements are admissible.

The remaining limitations are therefore methodological rather than missing implementation steps.

1. The compiled QAOA/VD/SV circuits are used in the validation layer, but the theorem-level implementation-noise model remains the idealized multiplicative baseline.
2. Level 2 and Level 3 use concrete QAOA families and readout-calibrated sector postselection, but they validate form and robustness rather than analytic coefficients.
3. The hardware conclusion concerns the global interferometric VD circuits implemented here. Localized virtual distillation, layout-aware compilation, or other lower-depth purification circuits can change implementation constants such as κ_M and move a crossing window; they do not remove the need to certify denominator concentration, quotient bias, and physical resource normalization.
4. CDR remains outside the theorem-level selector unless a separate training-model law is proved.
5. The hardware layer is qualitative and budget-limited: it uses three archived instances on a primary backend plus one independent cross-backend replicate of `g6_k2_c000`, with cluster bootstrap over calibration epochs, so it supports feasibility and robustness rather than a hardware-universal ordering.

15 Conclusion

The central message is that finite-shot error mitigation is a regime problem, not a one-number ranking. VD and SV can be compared by operating windows only after their residual bias floors, sampling coefficients, quotient corrections, and remainder regimes are explicit. In the closed one-qubit transcript, the selector can also be compared directly with conservative Le Cam and sharper local Fisher benchmarks; these are used as physical distinguishability limits for fixed noisy measurement transcripts, not as abstract statistical decoration. In the sector toy, the residual SV bias floor is compared with a restricted structural non-identifiability floor. For VD, the key object is the quotient law plus the denominator certificate. For SV, the key object is the projected first-order perturbation $P\Delta P - \rho_\star \text{Tr}(P\Delta P)$. Once each method has a certified law

$$\begin{aligned} \text{MSE}_m(p, R) &= b_m(p)^2 + \frac{s_m(p)}{R} + \rho_m(p, R), \\ |\rho_m(p, R)| &\leq \frac{C_m(p)}{R^2}, \end{aligned} \tag{124}$$

method selection becomes a lower-envelope problem with a self-consistency test for every crossing. This moves the comparison of mitigation methods from a purely formal Taylor framework to a mathematically defensible finite-budget theory. The three-level validation program supports that theory at the appropriate levels of claim: structural coefficient checks in the exact white-box Level 1 layer, form and robustness in the Aer Level 2 layer, and qualitative feasibility with calibrated readout on IBM hardware in Level 3.

Acknowledgements

The author thanks his parents, Luigi Stefano Scavino Montero and Isabel Betzabe Alfaro Ninahuanca, and his sister, Luciana Francesca Scavino Alfaro, for their constant support, patience, and encouragement throughout this work.

Author contribution statement

Vicenzo Scavino Alfaro is the sole author of this work and is responsible for the conceptual development, theoretical analysis, software, numerical and hardware-data analysis, validation, visualization, writing, and final approval of the manuscript.

The author used AI-assisted tools for editorial and workflow support. All scientific claims, calculations, code, data analysis, and manuscript text were reviewed and approved by the author, who remains fully responsible for the work.

References

- [1] Z. Cai, R. Babbush, S. C. Benjamin, S. Endo, W. J. Huggins, Y. Li, J. R. McClean, and T. E. O'Brien. Quantum error mitigation. *Reviews of Modern Physics*, 95:045005, 2023. doi:10.1103/RevModPhys.95.045005.
- [2] K. Temme, S. Bravyi, and J. M. Gambetta. Error mitigation for short-depth quantum circuits. *Physical Review Letters*, 119:180509, 2017. doi:10.1103/PhysRevLett.119.180509.
- [3] Y. Li and S. C. Benjamin. Efficient variational quantum simulator incorporating active error minimization. *Physical Review X*, 7:021050, 2017. doi:10.1103/PhysRevX.7.021050.
- [4] S. Endo, S. C. Benjamin, and Y. Li. Practical quantum error mitigation for near-future applications. *Physical Review X*, 8:031027, 2018. doi:10.1103/PhysRevX.8.031027.
- [5] X. Bonet-Monroig, R. Sagastizabal, M. Singh, and T. E. O'Brien. Low-cost error mitigation by symmetry verification. *Physical Review A*, 98:062339, 2018. doi:10.1103/PhysRevA.98.062339.
- [6] S. McArdle, X. Yuan, and S. Benjamin. Error-mitigated digital quantum simulation. *Physical Review Letters*, 122:180501, 2019. doi:10.1103/PhysRevLett.122.180501.
- [7] P. Czarnik, A. Arrasmith, P. J. Coles, and L. Cincio. Error mitigation with Clifford quantum-circuit data. *Quantum*, 5:592, 2021. doi:10.22331/q-2021-11-26-592.
- [8] A. Lowe, M. H. Gordon, P. Czarnik, A. Arrasmith, P. J. Coles, and L. Cincio. Unified approach to data-driven quantum error mitigation. *Physical Review Research*, 3:033098, 2021. doi:10.1103/PhysRevResearch.3.033098.
- [9] W. J. Huggins, S. McArdle, T. E. O'Brien, J. Lee, N. C. Rubin, S. Boixo, K. B. Whaley, R. Babbush, and J. R. McClean. Virtual distillation for quantum error mitigation. *Physical Review X*, 11:041036, 2021. doi:10.1103/PhysRevX.11.041036.
- [10] B. Koczor. Exponential error suppression for near-term quantum devices. *Physical Review X*, 11:031057, 2021. doi:10.1103/PhysRevX.11.031057.
- [11] M. Huo and Y. Li. Dual-state purification for practical quantum error mitigation. *Physical Review A*, 105:022427, 2022. doi:10.1103/PhysRevA.105.022427.
- [12] H. Hakoshima, S. Endo, K. Yamamoto, Y. Matsuzaki, and N. Yoshioka. Localized virtual purification. *Physical Review Letters*, 133:080601, 2024. doi:10.1103/PhysRevLett.133.080601.
- [13] X. Yuan, B. Regula, R. Takagi, and M. Gu. Virtual quantum resource distillation. *Physical Review Letters*, 132:050203, 2024. doi:10.1103/PhysRevLett.132.050203.
- [14] D. Bultrini, M. H. Gordon, P. Czarnik, A. Arrasmith, M. Cerezo, P. J. Coles, and L. Cincio. Unifying and benchmarking state-of-the-art quantum error mitigation techniques. *Quantum*, 7:1034, 2023. doi:10.22331/q-2023-06-06-1034.

- [15] A. Ijaz, C. Huerta Alderete, F. Sauvage, L. Cincio, M. Cerezo, and M. L. Goh. More buck-per-shot: Why learning trumps mitigation in noisy quantum sensing. *Materials Today Quantum*, 6:100042, 2025. doi:10.1016/j.mtquan.2025.100042.
- [16] B. Koczor. The dominant eigenvector of a noisy quantum state. *New Journal of Physics*, 23:123047, 2021. doi:10.1088/1367-2630/ac37ae.
- [17] R. Sagastizabal, X. Bonet-Monroig, M. Singh, M. A. Rol, C. C. Bultink, X. Fu, C. H. Price, V. P. Ostroukh, N. Muthusubramanian, A. Bruno, M. Beekman, N. Haider, T. E. O’Brien, and L. DiCarlo. Experimental error mitigation via symmetry verification in a variational quantum eigensolver. *Physical Review A*, 100:010302(R), 2019. doi:10.1103/PhysRevA.100.010302.
- [18] A. Kakkar, J. Larson, A. Galda, and R. Shaydulin. Characterizing error mitigation by symmetry verification in QAOA. In *2022 IEEE International Conference on Quantum Computing and Engineering (QCE)*, pages 306–316, 2022. doi:10.1109/QCE53715.2022.00086.
- [19] Z. Cai. Quantum error mitigation using symmetry expansion. *Quantum*, 5:548, 2021. doi:10.22331/q-2021-09-21-548.
- [20] Y. S. Teo, S. Shin, H. Kwon, S.-H. Lee, and H. Jeong. Virtual distillation with noise dilution. *Physical Review A*, 107:022608, 2023. doi:10.1103/PhysRevA.107.022608.
- [21] P. Vikstal, G. Ferrini, and S. Puri. Study of noise in virtual distillation circuits for quantum error mitigation. *Quantum*, 8:1441, 2024. doi:10.22331/q-2024-08-14-1441.
- [22] T. E. O’Brien et al. Purification-based quantum error mitigation of pair-correlated electron simulations. *Nature Physics*, 19:1787–1792, 2023. doi:10.1038/s41567-023-02240-y.
- [23] M. Demarty, B. Yang, K. Hammam, and P. Besserve. Error-mitigation aware benchmarking strategy for quantum optimization problems. arXiv:2601.18680, 2026. doi:10.48550/arXiv.2601.18680.
- [24] M. Seksaria and A. Prabhakar. Estimating shots and variance on noisy quantum circuits. arXiv:2501.03194, 2025. doi:10.48550/arXiv.2501.03194.
- [25] P. Niroula, S. Gopalakrishnan, and M. J. Gullans. Error mitigation thresholds in noisy random quantum circuits. *Physical Review B*, 112:024206, 2025. doi:10.1103/qsms-9kkh.
- [26] A. Javadi-Abhari et al. Quantum computing with Qiskit. arXiv:2405.08810, 2024. doi:10.48550/arXiv.2405.08810.
- [27] F. B. Maciejewski, Z. Zimboras, and M. Oszmaniec. Mitigation of readout noise in near-term quantum devices by classical post-processing based on detector tomography. *Quantum*, 4:257, 2020. doi:10.22331/q-2020-04-24-257.
- [28] S. Bravyi, S. Sheldon, A. Kandala, D. C. McKay, and J. M. Gambetta. Mitigating measurement errors in multiqubit experiments. *Physical Review A*, 103:042605, 2021. doi:10.1103/PhysRevA.103.042605.
- [29] W. G. Cochran. *Sampling Techniques*. Wiley, 3rd edition, 1977. ISBN 978-0-471-16240-7.
- [30] T. Kato. *Perturbation Theory for Linear Operators*. Springer, 1995. doi:10.1007/978-3-642-66282-9.
- [31] R. A. Horn and C. R. Johnson. *Matrix Analysis*. Cambridge University Press, 2nd edition, 2013. ISBN 978-0-521-83940-2.
- [32] S. Boucheron, G. Lugosi, and P. Massart. *Concentration Inequalities: A Nonasymptotic Theory of Independence*. Oxford University Press, 2013. doi:10.1093/acprof:oso/9780199535255.001.0001.

- [33] A. K. Ekert, C. M. Alves, D. K. L. Oi, M. Horodecki, P. Horodecki, and L. C. Kwak. Direct estimations of linear and nonlinear functionals of a quantum state. *Physical Review Letters*, 88:217901, 2002. doi:10.1103/PhysRevLett.88.217901.
- [34] E. van den Berg, Z. K. Mineev, A. Kandala, and K. Temme. Probabilistic error cancellation with sparse Pauli–Lindblad models on noisy quantum processors. *Nature Physics*, 19:1116–1121, 2023. doi:10.1038/s41567-023-02042-2.
- [35] R. Takagi, S. Endo, S. Minagawa, and M. Gu. Fundamental limits of quantum error mitigation. *npj Quantum Information*, 8:114, 2022. doi:10.1038/s41534-022-00618-z.
- [36] R. Takagi, H. Tajima, and M. Gu. Universal sampling lower bounds for quantum error mitigation. *Physical Review Letters*, 131:210602, 2023. doi:10.1103/PhysRevLett.131.210602.
- [37] K. Tsubouchi, T. Sagawa, and N. Yoshioka. Universal cost bound of quantum error mitigation based on quantum estimation theory. *Physical Review Letters*, 131:210601, 2023. doi:10.1103/PhysRevLett.131.210601.
- [38] Y. Quek, D. Stilck França, S. Khatri, J. J. Meyer, and J. Eisert. Exponentially tighter bounds on limitations of quantum error mitigation. *Nature Physics*, 20:1648–1658, 2024. doi:10.1038/s41567-024-02536-7.
- [39] L. Le Cam. Convergence of estimates under dimensionality restrictions. *The Annals of Statistics*, 1:38–53, 1973. doi:10.1214/aos/1193342380.
- [40] A. B. Tsybakov. *Introduction to Nonparametric Estimation*. Springer, 2009. doi:10.1007/b13794.
- [41] A. W. van der Vaart. *Asymptotic Statistics*. Cambridge University Press, 1998. doi:10.1017/CBO9780511802256.
- [42] E. Farhi, J. Goldstone, and S. Gutmann. A quantum approximate optimization algorithm. arXiv:1411.4028, 2014. doi:10.48550/arXiv.1411.4028.
- [43] S. Hadfield, Z. Wang, B. O’Gorman, E. G. Rieffel, D. Venturelli, and R. Biswas. From the quantum approximate optimization algorithm to a quantum alternating operator ansatz. *Algorithms*, 12:34, 2019. doi:10.3390/a12020034.
- [44] B. A. Nosek, C. R. Ebersole, A. C. DeHaven, and D. T. Mellor. The preregistration revolution. *Proceedings of the National Academy of Sciences*, 115:2600–2606, 2018. doi:10.1073/pnas.1708274114. doi:10.1002/pst.291.
- [45] H. Akaike. A new look at the statistical model identification. *IEEE Transactions on Automatic Control*, 19:716–723, 1974. doi:10.1109/TAC.1974.1100705.
- [46] K. P. Burnham and D. R. Anderson. *Model Selection and Multimodel Inference: A Practical Information-Theoretic Approach*. Springer, 2nd edition, 2002. doi:10.1007/b97636.
- [47] D. J. Schuirmann. A comparison of the two one-sided tests procedure and the power approach for assessing the equivalence of average bioavailability. *Journal of Pharmacokinetics and Biopharmaceutics*, 15:657–680, 1987. doi:10.1007/BF01068419.
- [48] T. Giurgica-Tiron, Y. Hindy, R. LaRose, A. Mari, and W. J. Zeng. Digital zero noise extrapolation for quantum error mitigation. In *2020 IEEE International Conference on Quantum Computing and Engineering (QCE)*, pages 306–316, 2020. doi:10.1109/QCE49297.2020.00045.
- [49] B. Efron and R. J. Tibshirani. *An Introduction to the Bootstrap*. Chapman and Hall/CRC, 1993. doi:10.1201/9780429246593.

A Quotient delta-method template

Let $(U_s, V_s)_{s=1}^B$ be i.i.d. with means (u, v) , $v > 0$, and covariance matrix

$$\Sigma = \begin{pmatrix} \sigma_U^2 & \sigma_{UV} \\ \sigma_{UV} & \sigma_V^2 \end{pmatrix}. \quad (\text{A.1})$$

Let $\hat{u} = B^{-1} \sum_s U_s$, $\hat{v} = B^{-1} \sum_s V_s$, and $\hat{\theta} = \hat{u}/\hat{v}$. With $\theta = u/v$,

$$\mathbb{E}\hat{\theta} = \theta + \frac{\theta\sigma_V^2 - \sigma_{UV}}{Bv^2} + \mathcal{R}_E(B), \quad (\text{A.2})$$

$$\text{Var}(\hat{\theta}) = \frac{\sigma_U^2 + \theta^2\sigma_V^2 - 2\theta\sigma_{UV}}{Bv^2} + \mathcal{R}_V(B), \quad (\text{A.3})$$

where, under the bounded-denominator conditions used in the body, $|\mathcal{R}_E(B)| \leq A_E/B^2 + E_{\text{bad}}(B)$ and $|\mathcal{R}_V(B)| \leq A_V/B^2 + V_{\text{bad}}(B)$. This is only the algebraic template behind VD and SV; it is the standard delta-method quotient expansion [41]. The certified versions in [Theorems 1](#) and [3](#) add denominator concentration and clipping to make the expansion non-asymptotically meaningful.

B Explicit quotient-remainder constants

This appendix assembles the explicit constants used in [Theorem 1](#), and, through the substitution stated there, in [Theorem 3](#).

Definition 2 (Explicit quotient-remainder constants). *For fixed (p, M) , put $\mu_M = N_M/D_M$. For sample means $\bar{\xi} = B^{-1} \sum_s \xi_s$ and $\bar{\zeta} = B^{-1} \sum_s \zeta_s$, define finite moment envelopes*

$$\mathbf{m}_{12,M}(p) = \sup_{B \geq 1} B^2 \left| \mathbb{E}[\bar{\xi} \bar{\zeta}^2] \right|, \quad \mathbf{m}_{21,M}(p) = \sup_{B \geq 1} B^2 \left| \mathbb{E}[\bar{\xi}^2 \bar{\zeta}] \right|, \quad (\text{B.1})$$

$$\mathbf{m}_{03,M}(p) = \sup_{B \geq 1} B^2 \left| \mathbb{E}[\bar{\zeta}^3] \right|, \quad \mathbf{m}_{13,M}(p) = \sup_{B \geq 1} B^2 \mathbb{E} \left[\left| \bar{\xi} \right| \left| \bar{\zeta} \right|^3 \right], \quad (\text{B.2})$$

$$\mathbf{m}_{04,M}(p) = \sup_{B \geq 1} B^2 \mathbb{E} \left[\left| \bar{\zeta} \right|^4 \right], \quad \mathbf{m}_{40,M}(p) = \sup_{B \geq 1} B^2 \mathbb{E} \left[\left| \bar{\xi} \right|^4 \right], \quad (\text{B.3})$$

$$\mathbf{m}_{22,M}(p) = \sup_{B \geq 1} B^2 \mathbb{E}[\bar{\xi}^2 \bar{\zeta}^2]. \quad (\text{B.4})$$

These constants are finite under [Assumption 1](#). For centered sample means the third-order envelopes satisfy the exact identities

$$\mathbf{m}_{12,M} = |m_{12,M}|, \quad \mathbf{m}_{21,M} = |m_{21,M}|, \quad \mathbf{m}_{03,M} = |m_{03,M}|,$$

because only the fully diagonal index contractions survive. A fully explicit admissible choice for the fourth-order envelopes follows from standard fourth-moment estimates for bounded centered averages; for example $\mathbf{m}_{04,M} \leq 3\sigma_{D,M}^4 + K_{D,M}^4$, $\mathbf{m}_{40,M} \leq 3\sigma_{N,M}^4 + 16K_{N,M}^4$, $\mathbf{m}_{22,M} \leq (3\sigma_{N,M}^4 + 16K_{N,M}^4)^{1/2} (3\sigma_{D,M}^4 + K_{D,M}^4)^{1/2}$.

For the variance certificate define the linear and quadratic quotient terms

$$L_M = \frac{\bar{\xi} - \mu_M \bar{\zeta}}{D_M}, \quad Q_M = \frac{\mu_M \bar{\zeta}^2 - \bar{\xi} \bar{\zeta}}{D_M^2}, \quad (\text{B.5})$$

put $G = \{|\bar{\zeta}| \leq D_M/2\}$, and let

$$T_M = \begin{cases} \frac{\bar{\xi}\bar{\zeta}^2 - \mu_M\bar{\zeta}^3}{D_M^3} - \frac{\bar{\xi}\bar{\zeta}^3}{D_M^4} + \frac{N_M + \bar{\xi}}{D_M} \frac{(\bar{\zeta}/D_M)^4}{1 + \bar{\zeta}/D_M}, & |\bar{\zeta}| \leq D_M/2, \\ 0, & |\bar{\zeta}| > D_M/2. \end{cases} \quad (\text{B.6})$$

Thus T_M is the signed sum of the third-and-higher Neumann terms after Q_M , restricted to the good event where the displayed tail is bounded. The remaining finite variance-tail envelope is

$$\mathfrak{t}_M^{(V)}(p) := \sup_{B \geq 1} B^2 |2 \text{Cov}(L_M, T_M) + 2 \text{Cov}(Q_M, T_M) + \text{Var}(T_M)|. \quad (\text{B.7})$$

It is finite under the boundedness assumption; if desired it can be expanded into sixth- and eighth-moment envelopes of $(\bar{\xi}, \bar{\zeta})$. Keeping it as $\mathfrak{t}_M^{(V)}$ avoids hiding the $\text{Cov}(L_M, T_M)$ term inside an informal $\mathcal{O}(B^{-2})$. Define

$$A_{E,M}(p) = \frac{\mathfrak{m}_{12,M}(p) + |\mu_M| \mathfrak{m}_{03,M}(p)}{D_M(p)^3} + \frac{\mathfrak{m}_{13,M}(p)}{D_M(p)^4} + \frac{2K_{N,M}(p)\mathfrak{m}_{04,M}(p)}{D_M(p)^5}, \quad (\text{B.8})$$

$$A_{Q,M}(p) = \frac{2}{D_M(p)^4} \left[|\mu_M|^2 \mathfrak{m}_{04,M}(p) + \mathfrak{m}_{22,M}(p) \right], \quad (\text{B.9})$$

$$A_{LQ,M}(p) = \frac{2}{D_M(p)^3} \left[2|\mu_M| \mathfrak{m}_{12,M}(p) + \mathfrak{m}_{21,M}(p) + |\mu_M|^2 \mathfrak{m}_{03,M}(p) \right], \quad (\text{B.10})$$

$$A_{V,M}(p) = A_{Q,M}(p) + A_{LQ,M}(p) + \mathfrak{t}_M^{(V)}(p), \quad (\text{B.11})$$

$$\omega_M(p) = \frac{K_{D,M}(p)}{D_M(p)}, \quad (\text{B.12})$$

$$B_{E,M}(p) = \frac{2K_{N,M}(p)}{D_M(p)} \left(5 + 3\omega_M(p) + 3\omega_M(p)^2 + 3\omega_M(p)^3 \right), \quad (\text{B.13})$$

$$B_{V,M}(p) = 2B_{E,M}(p)^2, \quad (\text{B.14})$$

$$E_{\text{bad},M}(p, B) = B_{V,M}(p) \exp \left[-\frac{BD_M(p)^2}{8\sigma_{D,M}^2(p) + \frac{4}{3}K_{D,M}(p)D_M(p)} \right]. \quad (\text{B.15})$$

The constants are conservative, and the mixed covariance between the linear and quadratic quotient terms is controlled explicitly. In particular, [Equation \(B.10\)](#) controls $2 \text{Cov}(L_M, Q_M)$, the term that is not controlled by bounding $\text{Var}(Q_M)$ alone.

We also record here the sharp asymptotic second-order variance coefficient of the clipped quotient, which identifies the moment combination that controls the true B^{-2} correction and explains why the worst-case envelope $A_{V,M}$ above is pessimistic.

Proposition B.1 (Second-order variance coefficient of the quotient). *Under [Assumption 1](#), let $\mu_M = N_M/D_M$, $\bar{\xi} = B^{-1} \sum_s \xi_s$, $\bar{\zeta} = B^{-1} \sum_s \zeta_s$, and define the linear and quadratic quotient terms*

$$L_M = \frac{\bar{\xi} - \mu_M\bar{\zeta}}{D_M}, \quad (\text{B.16})$$

$$Q_M = \frac{\mu_M\bar{\zeta}^2 - \bar{\xi}\bar{\zeta}}{D_M^2}. \quad (\text{B.17})$$

Then, on the good-denominator event and up to an exponentially small clipping correction,

$$\text{Var}(\widehat{\mu}_{\text{VD},M}^{\text{clip}}) = \frac{v_{\text{VD},M}}{B} + \frac{W_{\text{VD},M}^{(0)}}{B^2} + \mathcal{O}(B^{-3}) + \mathcal{O}(e^{-\gamma_M B}), \quad (\text{B.18})$$

where the exact third-moment contribution and the clean second-order coefficient are

$$\begin{aligned} \Gamma_{\text{VD},M} &:= \frac{2}{D_M^3} \left(2\mu_M m_{12,M} - m_{21,M} - \mu_M^2 m_{03,M} \right) \\ &= 2B^2 \text{Cov}(L_M, Q_M), \end{aligned} \quad (\text{B.19})$$

$$\begin{aligned} W_{\text{VD},M}^{(0)} &= \Gamma_{\text{VD},M} + \frac{1}{D_M^4} \left[8\mu_M^2 \sigma_{D,M}^4 + 3\sigma_{N,M}^2 \sigma_{D,M}^2 \right. \\ &\quad \left. + 5\sigma_{ND,M}^2 - 16\mu_M \sigma_{D,M}^2 \sigma_{ND,M} \right], \end{aligned} \quad (\text{B.20})$$

$$\begin{aligned} B^2 \text{Var}(Q_M) &= \frac{1}{D_M^4} \left[2\mu_M^2 \sigma_{D,M}^4 + \sigma_{N,M}^2 \sigma_{D,M}^2 \right. \\ &\quad \left. + \sigma_{ND,M}^2 - 4\mu_M \sigma_{D,M}^2 \sigma_{ND,M} \right] + \mathcal{O}(B^{-1}), \end{aligned} \quad (\text{B.21})$$

$$\begin{aligned} 2B^2 \text{Cov}(L_M, T_M^{(3)}) &= \frac{2}{D_M^4} \left[3\mu_M^2 \sigma_{D,M}^4 + \sigma_{N,M}^2 \sigma_{D,M}^2 \right. \\ &\quad \left. + 2\sigma_{ND,M}^2 - 6\mu_M \sigma_{D,M}^2 \sigma_{ND,M} \right] + \mathcal{O}(B^{-1}). \end{aligned} \quad (\text{B.22})$$

where $T_M^{(3)} = (\bar{\xi}^2 - \mu_M \bar{\zeta}^3) / D_M^3$. The term $\Gamma_{\text{VD},M}$ is the exact third-moment contribution from $2 \text{Cov}(L_M, Q_M)$. For the independent Hadamard-test implementation used below, $m_{12,M} = m_{21,M} = 0$ and $m_{03,M} = -2D_M(1 - D_M^2)$, hence

$$\Gamma_{\text{VD},M}^{\text{Had}} = \frac{4\mu_M^2(1 - D_M^2)}{D_M^2}. \quad (\text{B.23})$$

Thus $\Gamma_{\text{VD},M}$ vanishes only in special cases such as $\mu_M = 0$ or $D_M = 1$; no such cancellation is assumed in the non-asymptotic certificate.

The proof, by direct contraction counting for centered sample averages, is given in [Section C](#).

Remark 10 (How this changes the interpretation of the toy certificates). [Lemma 3](#) and [Proposition B.1](#) do not change the leading operating-window law. They explain why the explicit constants used in the certified toy examples are pessimistic: $A_{V,M}$ is a worst-case certificate for a second-order remainder, whereas the actual B^{-2} variance correction is controlled by the full coefficient $W_{\text{VD},M}^{(0)}$ in [Equation \(B.20\)](#), including $\Gamma_{\text{VD},M}$ and the linear-cubic covariance. Thus the earlier extreme numerical choices demonstrate formal non-vacuity of the certificate; they do not indicate the physical scale at which VD or SV becomes useful.

C Deferred proofs

This appendix contains the proofs of [Theorem 1](#), [Proposition B.1](#), [Lemma D.1](#), and [Proposition D.7](#).

Proof of Theorem 1. Let $G = \{|\bar{\zeta}| \leq D_M/2\}$. On G , clipping is inactive and $\widehat{D}_M \geq D_M/2$. The centered variables satisfy $|N_M + \bar{\xi}| = |\widehat{N}_M| \leq K_{N,M}$. Since $|\bar{\zeta}/D_M| \leq 1/2$, the Neumann expansion is absolutely convergent and

$$\frac{1}{D_M + \bar{\zeta}} = \frac{1}{D_M} \left(1 - \frac{\bar{\zeta}}{D_M} + \frac{\bar{\zeta}^2}{D_M^2} - \frac{\bar{\zeta}^3}{D_M^3} \right) + \frac{1}{D_M} \frac{(\bar{\zeta}/D_M)^4}{1 + \bar{\zeta}/D_M}. \quad (\text{C.1})$$

Multiplying by $N_M + \bar{\xi} = \mu_M D_M + \bar{\xi}$ gives the term-by-term identity

$$\frac{N_M + \bar{\xi}}{D_M + \bar{\zeta}} = \mu_M + \frac{\bar{\xi} - \mu_M \bar{\zeta}}{D_M} + \frac{\mu_M \bar{\zeta}^2 - \bar{\xi} \bar{\zeta}}{D_M^2} + \frac{\bar{\xi} \bar{\zeta}^2 - \mu_M \bar{\zeta}^3}{D_M^3} - \frac{\bar{\xi} \bar{\zeta}^3}{D_M^4} + \widetilde{\mathcal{R}}_4, \quad (\text{C.2})$$

where

$$\widetilde{\mathcal{R}}_4 = \frac{N_M + \bar{\xi}}{D_M} \frac{(\bar{\zeta}/D_M)^4}{1 + \bar{\zeta}/D_M}. \quad (\text{C.3})$$

The good-event tail is therefore explicitly bounded by

$$|\widetilde{\mathcal{R}}_4| \leq \frac{2K_{N,M} |\bar{\zeta}|^4}{D_M^5}. \quad (\text{C.4})$$

The mixed cubic term $-\bar{\xi} \bar{\zeta}^3/D_M^4$ is kept separate so that the remaining tail contains only powers $\bar{\zeta}^4$ and higher. Taking expectations of the unrestricted monomials through second order, using $\mathbb{E}\bar{\xi} = \mathbb{E}\bar{\zeta} = 0$, $\mathbb{E}\bar{\zeta}^2 = \sigma_{D,M}^2/B$, and $\mathbb{E}\bar{\xi}\bar{\zeta} = \sigma_{ND,M}/B$, gives the coefficient $c_{VD,M}/B$. The cubic, mixed cubic, and geometric-tail terms are bounded by $A_{E,M}/B^2$ from the definitions of $\mathfrak{m}_{12}, \mathfrak{m}_{03}, \mathfrak{m}_{13}, \mathfrak{m}_{04}$. Restoring the restriction to G changes each bounded monomial expectation by at most its uniform bound times $\mathbb{P}(G^c)$, and on G^c the clipped estimator obeys $|\widehat{\mu}_{VD,M}^{\text{clip}}| \leq 2K_{N,M}/D_M$. The prefactor $B_{E,M}$ in Definition 2 collects these bad-event corrections, while Lemma 2 supplies the exponential probability. This proves Equation (37).

For the variance, set

$$Z_M = \mu_M + L_M + Q_M + T_M, \quad L_M = \frac{\bar{\xi} - \mu_M \bar{\zeta}}{D_M}, \quad Q_M = \frac{\mu_M \bar{\zeta}^2 - \bar{\xi} \bar{\zeta}}{D_M^2}, \quad (\text{C.5})$$

where T_M is the good-event third-and-higher tail in Equation (B.6). On G , $Z_M = \widehat{\mu}_{VD,M}^{\text{clip}}$. Put $W_M = \widehat{\mu}_{VD,M}^{\text{clip}} - Z_M$, so W_M is supported on G^c . Let $\omega_M = K_{D,M}/D_M$ and $P_M = 5 + 3\omega_M + 3\omega_M^2 + 3\omega_M^3$. Using $\text{Var}(Z_M + W_M) - \text{Var}(Z_M) = \text{Var}(W_M) + 2\text{Cov}(Z_M, W_M)$, the event-local sup-norm bookkeeping used in $B_{E,M}$ gives

$$\begin{aligned} |\text{Var}(Z_M + W_M) - \text{Var}(Z_M)| &\leq 6 \left(\frac{K_{N,M}}{D_M} \right)^2 P_M^2 \exp \left[-\frac{BD_M^2}{8\sigma_{D,M}^2 + \frac{4}{3}K_{D,M}D_M} \right] \\ &\leq 2B_{E,M}^2 \exp \left[-\frac{BD_M^2}{8\sigma_{D,M}^2 + \frac{4}{3}K_{D,M}D_M} \right] = E_{\text{bad},M}. \end{aligned} \quad (\text{C.6})$$

For Z_M , $B \text{Var}(L_M) = v_{VD,M}$. The quadratic variance term obeys

$$B^2 \text{Var}(Q_M) \leq B^2 \mathbb{E}[Q_M^2] \leq A_{Q,M}. \quad (\text{C.7})$$

The mixed linear-quadratic term is controlled explicitly by

$$2B^2 |\text{Cov}(L_M, Q_M)| \leq \frac{2B^2}{D_M^3} \left| \mathbb{E}[(\bar{\xi} - \mu_M \bar{\zeta})(\mu_M \bar{\zeta}^2 - \bar{\xi} \bar{\zeta})] \right| \quad (\text{C.8})$$

$$\leq \frac{2}{D_M^3} \left[2 |\mu_M| \mathbf{m}_{12,M} + \mathbf{m}_{21,M} + |\mu_M|^2 \mathbf{m}_{03,M} \right] = A_{LQ,M}. \quad (\text{C.9})$$

Finally, the remaining third-and-higher contributions are exactly those collected in $\mathbf{t}_M^{(V)}$. Therefore

$$|\text{Var}(Z_M) - \text{Var}(L_M)| \leq \frac{A_{Q,M} + A_{LQ,M} + \mathbf{t}_M^{(V)}}{B^2}, \quad (\text{C.10})$$

and the supported-on- G^c difference between Z_M and the clipped quotient is bounded by Equation (C.6). This proves Equation (38) and controls the covariance term that bounding $\text{Var}(Q_M)$ alone would not capture. The MSE expansion follows by combining the variance bound with

$$\left(b_{\text{VD},M} + \frac{c_{\text{VD},M}}{B} + r_M^{(E)} \right)^2 = b_{\text{VD},M}^2 + \frac{2b_{\text{VD},M}c_{\text{VD},M}}{B} + \mathcal{O}(B^{-2}), \quad (\text{C.11})$$

where the $\mathcal{O}(B^{-2})$ term is replaced by the explicit bounds above in Equation (40). \square

Proof of Proposition B.1. Use the Neumann expansion of $(D_M + \bar{\zeta})^{-1}$ on the event $|\bar{\zeta}| \leq D_M/2$:

$$\frac{N_M + \bar{\xi}}{D_M + \bar{\zeta}} = \mu_M + L_M + Q_M + T_M^{(3)} + \mathcal{O}\left(|\bar{\xi}| |\bar{\zeta}|^3 + |\bar{\zeta}|^4\right), \quad T_M^{(3)} = \frac{\bar{\xi} \bar{\zeta}^2 - \mu_M \bar{\zeta}^3}{D_M^3}. \quad (\text{C.12})$$

The leading term satisfies $B \text{Var}(L_M) = v_{\text{VD},M}$. For centered i.i.d. sample averages,

$$\text{Var}(\bar{\zeta}^2) = \frac{2\sigma_{D,M}^4}{B^2} + \mathcal{O}(B^{-3}), \quad (\text{C.13})$$

$$\text{Var}(\bar{\xi} \bar{\zeta}) = \frac{\sigma_{N,M}^2 \sigma_{D,M}^2 + \sigma_{ND,M}^2}{B^2} + \mathcal{O}(B^{-3}), \quad (\text{C.14})$$

$$\text{Cov}(\bar{\zeta}^2, \bar{\xi} \bar{\zeta}) = \frac{2\sigma_{D,M}^2 \sigma_{ND,M}}{B^2} + \mathcal{O}(B^{-3}). \quad (\text{C.15})$$

Substituting these three identities into $Q_M = (\mu_M \bar{\zeta}^2 - \bar{\xi} \bar{\zeta})/D_M^2$ gives Equation (B.21). The covariance $\text{Cov}(L_M, Q_M)$ contains third moments; the exact contraction identity

$$\mathbb{E}\left[(\bar{\xi} - \mu_M \bar{\zeta})(\mu_M \bar{\zeta}^2 - \bar{\xi} \bar{\zeta})\right] = \frac{2\mu_M m_{12,M} - m_{21,M} - \mu_M^2 m_{03,M}}{B^2}$$

gives Equation (B.19). The cubic term cannot be discarded at second order, because $\text{Var}(T_M^{(3)}) = \mathcal{O}(B^{-3})$ but $\text{Cov}(L_M, T_M^{(3)}) = \mathcal{O}(B^{-2})$. Writing $A_s = \xi_s - \mu_M \zeta_s$, a direct contraction count for centered i.i.d. averages gives

$$B^2 \mathbb{E}[\bar{A}^2 \bar{\zeta}^2] = \text{Var}(A_s) \sigma_{D,M}^2 + 2 \text{Cov}(A_s, \zeta_s)^2 + \mathcal{O}(B^{-1}), \quad (\text{C.16})$$

which is Equation (B.22). All fourth-and-higher Neumann terms have only $\mathcal{O}(B^{-3})$ covariance with L_M ; boundedness in Assumption 1 supplies the finite sixth moments needed for these constants and gives the exponentially small clipping correction through Lemma 2. \square

Proof of Lemma D.1. On \mathcal{G} ,

$$\frac{\bar{Z}}{\bar{A}} = \frac{\bar{z}}{a} \sum_{k=0}^{\infty} \left(-\frac{\bar{\alpha}}{a}\right)^k, \quad |\bar{\alpha}/a| \leq \frac{1}{2}. \quad (\text{C.17})$$

Therefore the post-quadratic remainder is

$$H_{\text{SV}} := \frac{\bar{Z}}{\bar{A}} - L_{\text{SV}} - Q_{\text{SV}} = \frac{\bar{z}\bar{\alpha}^2}{a^3} \frac{1}{1 + \bar{\alpha}/a}, \quad (\text{C.18})$$

and $|H_{\text{SV}}| \leq 16|\bar{z}|\bar{\alpha}^2$. We now spell out the only contraction structure used in the displayed bound. Since $Z_s A_s = Z_s$, $Z_s = 0$ on rejection, and $\mathbb{E}Z_s = 0$, one has

$$\mathbb{E}[Z_s(A_s - a)^r] = (1 - a)^r \mathbb{E}Z_s = 0, \quad r = 0, 1, 2, 3, 4. \quad (\text{C.19})$$

Thus any sample-index block containing a single Z and any number of $\alpha = A - a$ factors vanishes. In the expansion of $\bar{z}^2\bar{\alpha}^4$, the two Z -indices must therefore coincide; after this identification, every remaining sample index carrying only α -factors must occur with multiplicity at least two, because $\mathbb{E}(A_s - a) = 0$. The surviving partitions are consequently only $\{ZZ\}\{\alpha\alpha\}\{\alpha\alpha\}$, $\{ZZ\alpha\}\{\alpha\alpha\alpha\}$, $\{ZZ\alpha\alpha\}\{\alpha\alpha\}$, and $\{ZZ\alpha\alpha\alpha\}$, together with index coincidences among these blocks. Using $Z_s^2 \leq A_s$, $|A_s - a| \leq 1$, and $a \geq 1/2$, this finite enumeration gives

$$\mathbb{E}[\bar{z}^2\bar{\alpha}^4] \leq \frac{1}{32R^2}. \quad (\text{C.20})$$

Combining the previous two displays gives [Equation \(D.39\)](#). Finally, on \mathcal{G}^c the clipped quotient contribution is bounded by $4\mathbb{P}(\mathcal{G}^c) \leq 8e^{-R/16}$; the stated slightly looser absorption $16e^{-R/16} \leq 2/R^2$ leaves room for the post-quadratic expectation/variance cross terms involving H_{SV} and the bad-event correction. Thus $8/R^2 + 2/R^2 = 10/R^2$, proving the claimed post-quadratic envelope. \square

Proof of [Proposition D.7](#). For $u = \ell = 1$ and $p = 10^{-2}$,

$$D_2 = (1 - 2p)^2 + p^2 + p^2 = 0.9606 > 0.96. \quad (\text{C.21})$$

With $K_{N,2} = 1$ and $K_{D,2} = 2$, [Equation \(44\)](#) gives

$$\frac{8K_{N,2}^2(D_2 + 2K_{D,2})^2}{D_2^4} \leq \frac{8(1 + 4)^2}{0.96^4} < 236, \quad (\text{C.22})$$

which gives $\text{Var}(\hat{\mu}_{\text{VD},2}^{\text{clip}}) \leq 236/B = 472/R$ because $B = R/2$. This proves [Equation \(D.81\)](#). The exact VD population bias in the sector toy is

$$b_{\text{VD},2}(p) = -\frac{(2u^2 + \ell^2)p^2}{D_2(p)}, \quad (\text{C.23})$$

so $|b_{\text{VD},2}| \leq 3p^2/0.96 < 4p^2$. The SV bias is

$$b_{\text{SV}}(p) = -\frac{2up}{1 - \ell p}. \quad (\text{C.24})$$

Here $u = \ell = 1$ and $p = 10^{-2} < 1$, so $0 < 1 - \ell p < 1$. Hence

$$b_{\text{SV}}(p)^2 = \frac{4p^2}{(1 - p)^2} > 4p^2. \quad (\text{C.25})$$

Numerically this is $4.0812\dots \times 10^{-4}$, safely above 4.0×10^{-4} ; the inequality follows from the denominator $1 - p < 1$, not from rounding. The finite-shot SV expectation correction is much smaller than this margin:

$$\varepsilon_{\text{SV,sector}}^{(E)}(R) < 10^{-9} \ll |b_{\text{SV}}(p)| - 2p, \quad (\text{C.26})$$

using $a = 0.99$, $|Z| \leq 1$, and the explicit Bernoulli quotient constants, including the exponentially small bad-event term, in [Theorem 3](#). Therefore

$$\left(|b_{\text{SV}}(p)| - \varepsilon_{\text{SV,sector}}^{(E)}(R)\right)^2 \geq 4p^2,$$

which proves [Equation \(D.83\)](#). It remains to justify the displayed $4/R$ finite-sample quotient-bias allowance for VD. In this independent Hadamard-test implementation $\sigma_{ND} = 0$ and the denominator sign has variance $\sigma_D^2 = 1 - D_2^2$. Hence

$$\frac{|c_{\text{VD},2}|}{B} = \frac{|\mu_{\text{VD},2}| \sigma_D^2}{D_2^2 B} \leq \frac{1 - D_2^2}{D_2^2 B} < \frac{0.09}{B} < \frac{4}{R}. \quad (\text{C.27})$$

The remaining expectation remainder is controlled by [Equation \(E.4\)](#):

$$\frac{A_{E,\text{VD},2}^{\text{sector}}}{B^2} < \frac{3.1 \times 10^3}{(10^6)^2} < 3.1 \times 10^{-9}. \quad (\text{C.28})$$

For the denominator event, [Equation \(E.10\)](#) gives $B_{\text{den},2} \leq 31 \log(2 \times 10^6) < 4.5 \times 10^2$ at failure probability 10^{-6} , while here $B = 10^6$; hence the exponentially small denominator contribution is also absorbed below 10^{-8} . Substituting $p = 10^{-2}$ and $R = 2 \times 10^6$ yields [Equation \(D.84\)](#). \square

D Toy model with closed constants and finite- p boundary

We first record the explicit lower-bound constants and the transcript-level efficiency statement that this appendix uses throughout; both instantiate [Theorem 6](#).

Proposition D.1 (Explicit I_p for a one-qubit Bernoulli transcript). *Consider the restricted local model*

$$\rho_t^* = \frac{I + tX}{2}, \quad \rho_{p,t} = \frac{I + (1-p)tX}{2}, \quad \mu_t^* = t, \quad (\text{D.1})$$

with $t \in [-t_0, t_0]$ and one resource unit equal to one noisy X -measurement. For the two hypotheses $t = \pm h$, the one-shot transcript distributions are Bernoulli distributions with means $\pm(1-p)h$ on $\{\pm 1\}$, and for $|h| \leq [2(1-p)]^{-1}$,

$$\text{KL}(P_{+h} \| P_{-h}) \leq 4(1-p)^2 h^2. \quad (\text{D.2})$$

Thus [Equation \(118\)](#) holds with the explicit conservative per-resource information constant

$$I_p^{\text{Bern}} = 4(1-p)^2. \quad (\text{D.3})$$

Consequently every estimator based on R such shots obeys the concrete lower bound

$$\sup_{t \in \{+h, -h\}} \mathbb{E}_t[(\hat{\mu} - t)^2] \geq \frac{1}{32R(1-p)^2}, \quad (\text{D.4})$$

provided the optimizing $h = [2RI_p^{\text{Bern}}]^{-1/2}$ lies in the local interval.

Proof. For $Y \in \{\pm 1\}$, write

$$q_+ = \frac{1+a}{2}, \quad q_- = \frac{1-a}{2}, \quad a = (1-p)h. \quad (\text{D.5})$$

In this symmetric two-point model $q_- = 1 - q_+$, which is the only reason the following simplification is valid. The Bernoulli KL is

$$\text{KL}(P_{+h}\|P_{-h}) = q_+ \log \frac{q_+}{q_-} + (1 - q_+) \log \frac{1 - q_+}{1 - q_-} \quad (\text{D.6})$$

$$= (2q_+ - 1) \log \frac{q_+}{1 - q_+} = a \log \frac{1 + a}{1 - a}. \quad (\text{D.7})$$

For $|a| \leq 1/2$, $|\log[(1 + a)/(1 - a)]| \leq 4|a|$, hence $a \log[(1 + a)/(1 - a)] \leq 4a^2$ and the KL is at most $4a^2$. This gives the conservative finite-interval value $I_p^{\text{Bern}} = 4(1 - p)^2$. The same expression also gives the sharper local constant: since $\log[(1 + a)/(1 - a)] = 2a + O(a^3)$,

$$\text{KL}(P_{+h}\|P_{-h}) = 2(1 - p)^2 h^2 + O(h^4), \quad (\text{D.8})$$

so the local two-point/Fisher normalization is

$$I_{p,\text{loc}}^{\text{Bern}} = 2(1 - p)^2. \quad (\text{D.9})$$

Equivalently, using $|\log[(1 + a)/(1 - a)]| \leq 2|a|/(1 - a^2)$ gives $I_p^{\text{Bern}} = 2(1 - p)^2/(1 - a^2)$, which tends to Equation (D.9) as $a \rightarrow 0$. Below we keep the conservative finite-interval value when a uniform certificate is needed and separately record the sharper local benchmark when comparing constants. \square

Proposition D.2 (Accepted-transcript efficiency of the selected law). *Fix p and suppose method m operates in a bias-negligible regime, meaning $b_m(p) = o(R^{-1/2})$ on the budget range under consideration, so that*

$$\text{MSE}_m(p, R) = \frac{s_m(p)}{R} + o(R^{-1}). \quad (\text{D.10})$$

Assume the per-resource transcript actually used by method m is a regular local statistical experiment with Fisher information $J_m(p)$ for the corresponding population value. Then

$$s_m(p) \geq \frac{1}{J_m(p)}. \quad (\text{D.11})$$

Equality holds when the method's estimator is locally efficient for that transcript. In the Pauli/Bernoulli accepted transcript used in the SV toy models, where each accepted observation has conditional variance $\sigma_{\text{acc}}^2(p)$ for the local mean parameter and acceptance probability $a(p)$,

$$J_{\text{SV}}(p) = \frac{a(p)}{\sigma_{\text{acc}}^2(p)}, \quad s_{\text{SV}}(p) = \frac{\sigma_{\text{acc}}^2(p)}{a(p)} = \frac{1}{J_{\text{SV}}(p)}. \quad (\text{D.12})$$

For a non-Bernoulli or non-efficient accepted transcript, Equation (D.12) should be read as an additional local-efficiency assumption, not as a universal identity. Thus the constant-factor gaps in the two-point Le Cam comparisons below are artifacts of conservative two-point testing only after the transcript model has been fixed.

Proof. Over R resource units the transcript has Fisher information $RJ_m(p)$. The local Cramer–Rao inequality [41] gives $\text{Var}(\hat{\mu}_m) \geq 1/[RJ_m(p)]$ for locally unbiased regular estimators, yielding Equation (D.11). For the Pauli/Bernoulli SV transcript, the number of accepted samples is $N_{\text{acc}} = \sum_{r=1}^R A_r$ with $A_r \sim \text{Bernoulli}(a(p))$. The same multiplicative Chernoff bound used in Theorem 3 gives, for every $0 < \delta < 1$,

$$\mathbb{P}(|N_{\text{acc}} - a(p)R| \geq \delta a(p)R) \leq 2 \exp[-a(p)R\delta^2/3]. \quad (\text{D.13})$$

Thus $N_{\text{acc}} = a(p)R + O_{\mathbb{P}}(\sqrt{R})$. Conditional on acceptance, the accepted Pauli/mean transcript has local information $1/\sigma_{\text{acc}}^2(p)$ per accepted observation, and the sample mean over accepted observations is locally efficient in this one-dimensional mean experiment. Hence the accepted transcript has Fisher information $a(p)R/\sigma_{\text{acc}}^2(p) + o(R)$, and its leading variance coefficient is $\sigma_{\text{acc}}^2(p)/a(p)$. This proves Equation (D.12) in the stated Pauli/Bernoulli setting and avoids asserting the identity for arbitrary accepted variables. \square

Remark 11 (Role relative to the Le Cam comparison). *The lower bound in Theorem 6 is a restricted two-point benchmark. Proposition D.2 is a sharper statement for the transcript actually used by SV in the bias-negligible regime. Both are useful, but they answer different questions: Le Cam tests whether any estimator can distinguish two nearby ideal targets from noisy data, while accepted-transcript efficiency tests whether a chosen postselected estimator wastes information inside its declared transcript.*

This section gives a minimal analytic example. It is not intended as a realistic benchmark; it demonstrates that the constants and validity certificates are computable on a finite interval, not only as formal Taylor coefficients.

Let the ideal one-qubit state be $\rho_{\star} = |0\rangle\langle 0|$, the observable be $O = X$, so $\mu_{\star} = 0$, and let the noisy state have spectral form

$$\rho_p = (1 - \varepsilon p) |\phi_1(p)\rangle\langle \phi_1(p)| + \varepsilon p |\phi_2(p)\rangle\langle \phi_2(p)|, \quad (\text{D.14})$$

where

$$|\phi_1(p)\rangle = \cos(\theta p) |0\rangle + \sin(\theta p) |1\rangle, \quad |\phi_2(p)\rangle = -\sin(\theta p) |0\rangle + \cos(\theta p) |1\rangle. \quad (\text{D.15})$$

Assume $\varepsilon > 0$, $\theta \neq 0$, and $0 < p \leq p_{\text{max}}$, where

$$p_{\text{max}} \leq \min \left\{ \frac{1}{4\varepsilon}, \frac{1}{4|\theta|} \right\}. \quad (\text{D.16})$$

This keeps the spectrum ordered and the trigonometric expansions uniformly controlled.

Unmitigated estimator. Since $\langle \phi_1 | X | \phi_1 \rangle = \sin(2\theta p)$ and $\langle \phi_2 | X | \phi_2 \rangle = -\sin(2\theta p)$,

$$\mu_0(p) = (1 - 2\varepsilon p) \sin(2\theta p). \quad (\text{D.17})$$

Using $|\sin x - x| \leq |x|^3/6$, $|2\theta p| \leq 1/2$, and $1 - 2\varepsilon p \geq 1/2$, the unmitigated squared bias obeys the finite-interval bounds

$$\frac{1}{2}\theta^2 p^2 \leq b_0(p)^2 \leq 16\theta^2 p^2 \quad (0 < p \leq p_{\text{max}}). \quad (\text{D.18})$$

Indeed, the sharper lower constant 529/576 also follows from $|\sin x| \geq (23/24)|x|$ on $|x| \leq 1/2$, but the displayed 1/2 is used below to keep the crossing certificate conservative. The one-shot variance for measuring X is

$$\sigma_0^2(p) = 1 - \mu_0(p)^2, \quad (\text{D.19})$$

and hence

$$1 - 16\theta^2 p_{\text{max}}^2 \leq \sigma_0^2(p) \leq 1. \quad (\text{D.20})$$

Virtual distillation. For $M \geq 2$,

$$\mu_{\text{VD},M}(p) = \frac{(1 - \varepsilon p)^M - (\varepsilon p)^M}{(1 - \varepsilon p)^M + (\varepsilon p)^M} \sin(2\theta p). \quad (\text{D.21})$$

The dominant-eigenvector floor is

$$b_{\text{VD},\infty}(p) = \sin(2\theta p) = 2\theta p + \mathcal{O}(p^3), \quad (\text{D.22})$$

so $\delta_{\text{VD}} = 2\theta$. VD cannot remove this coherent eigenvector mismatch. The denominator is

$$D_M(p) = (1 - \varepsilon p)^M + (\varepsilon p)^M. \quad (\text{D.23})$$

For $p \leq p_{\max}$,

$$(1 - \varepsilon p)^M \leq D_M(p) \leq (1 - \varepsilon p)^M \left[1 + \left(\frac{\varepsilon p}{1 - \varepsilon p} \right)^M \right]. \quad (\text{D.24})$$

The Hadamard denominator threshold [Equation \(52\)](#) is therefore explicit in $(\varepsilon, \theta, p, M)$.

Symmetry verification. Let $P = |0\rangle\langle 0|$. In this first toy, X is not a symmetry-compatible observable in the usual sense because $XP \neq PX$. The construction is an algebraic accepted-transcript quotient used to test the finite-shot crossing constants, not a complete physical SV protocol. The physically sector-compatible comparison is given in the next toy model. Then

$$a(p) = \text{Tr}(P\rho_p) = (1 - \varepsilon p) \cos^2(\theta p) + \varepsilon p \sin^2(\theta p). \quad (\text{D.25})$$

For $p \leq p_{\max}$,

$$\frac{11}{16} \leq a(p) \leq 1. \quad (\text{D.26})$$

Indeed, $1 - a(p) = \sin^2(\theta p) + \varepsilon p \cos(2\theta p) \leq \theta^2 p^2 + \varepsilon p \leq 5/16$. Moreover,

$$\mu_{\text{SV}}(p) = \frac{\text{Tr}(XP\rho_p P)}{a(p)} = 0, \quad (\text{D.27})$$

so $\delta_{\text{SV}} = 0$. If the accepted conditional X -measurement variance is one, then

$$s_{\text{SV}}(p) = \frac{1}{a(p)}, \quad 1 \leq s_{\text{SV}}(p) \leq 2. \quad (\text{D.28})$$

Toy remainder envelope. For this first toy model, the unmitigated estimator is the ordinary sample mean of a $\{\pm 1\}$ -valued variable. Hence its expectation and variance are exactly

$$\mathbb{E}\hat{\mu}_0 = \mu_0, \quad \text{Var}(\hat{\mu}_0) = \sigma_0^2/B, \quad (\text{D.29})$$

so the unmitigated R^{-2} coefficient is

$$C_{0,\text{toy}} = 0. \quad (\text{D.30})$$

For SV, the worst-case constants from the general quotient certificate are loose by design. In this first toy we compute the relevant second-order remainder directly. Let

$$Z_s = A_s X_s, \quad A_s \in \{0, 1\}, \quad \hat{\mu}_{\text{SV}} = \frac{\bar{Z}}{\bar{A}}, \quad (\text{D.31})$$

where A_s is the symmetry-acceptance indicator and $X_s \in \{\pm 1\}$ is the accepted X -measurement sign. In this toy, $\mu_{\text{SV}} = 0$, $\mathbb{E}Z_s = 0$, $\mathbb{E}A_s = a$, and

$$\sigma_Z^2 = a, \quad \sigma_A^2 = a(1-a), \quad \sigma_{ZA} = 0. \quad (\text{D.32})$$

Writing $\bar{z} = \bar{Z}$ and $\bar{\alpha} = \bar{A} - a$, the Neumann expansion gives

$$\frac{\bar{Z}}{\bar{A}} = L_{\text{SV}} + Q_{\text{SV}} + T_{\text{SV}}^{(3)} + \text{higher order}, \quad L_{\text{SV}} = \frac{\bar{z}}{a}, \quad Q_{\text{SV}} = -\frac{\bar{z}\bar{\alpha}}{a^2}, \quad T_{\text{SV}}^{(3)} = \frac{\bar{z}\bar{\alpha}^2}{a^3}. \quad (\text{D.33})$$

A direct calculation of the sample-average moments gives the asymptotic second-order coefficient

$$B^2 \text{Var}(Q_{\text{SV}}) = \frac{1-a}{a^2} + \mathcal{O}(B^{-1}), \quad (\text{D.34})$$

$$2B^2 \text{Cov}(L_{\text{SV}}, Q_{\text{SV}}) = -\frac{2(1-a)}{a^2}, \quad (\text{D.35})$$

$$2B^2 \text{Cov}(L_{\text{SV}}, T_{\text{SV}}^{(3)}) = \frac{2(1-a)}{a^2} + \mathcal{O}(B^{-1}). \quad (\text{D.36})$$

Thus the second-order asymptotic variance coefficient is

$$W_{\text{SV}} = \frac{1-a}{a^2}, \quad |W_{\text{SV}}| \leq 2 \quad \text{whenever } a \geq \frac{1}{2}. \quad (\text{D.37})$$

Because $Z \in \{-1, 0, 1\}$, $A \in \{0, 1\}$, and $a \geq 1/2$, the cubic and higher Neumann terms can be bounded directly rather than by the general worst-case SV quotient certificate.

Lemma D.1 (Direct SV toy remainder envelope). *In the first toy model, assume $a \geq 1/2$ and let $R = B$ be the accepted-transcript shot budget. On the good event*

$$\mathcal{G} = \{|\bar{A} - a| \leq a/2\}, \quad (\text{D.38})$$

the Neumann remainder after the linear and quadratic terms satisfies

$$\mathbb{E} \left[\mathbf{1}_{\mathcal{G}} \left(\frac{\bar{Z}}{\bar{A}} - L_{\text{SV}} - Q_{\text{SV}} \right)^2 \right] \leq \frac{8}{R^2}. \quad (\text{D.39})$$

Moreover, a two-sided Bernstein/Hoeffding bound [32] for the Bernoulli acceptance average gives

$$\mathbb{P}(\mathcal{G}^c) \leq 2e^{-R/16}, \quad (\text{D.40})$$

and the clipped quotient is bounded by 2 on \mathcal{G}^c . Hence, once $R \geq R_{\min, \text{toy}}$ is chosen so that $16e^{-R/16} \leq 2/R^2$, the total additional contribution of the post-quadratic Neumann terms and the bad-denominator event is bounded by $10/R^2$.

The proof, a finite enumeration of the surviving contraction partitions together with a Hoeffding bound for the bad event, is given in [Section C](#).

Consequently, for the certified toy crossing on budgets $R \geq R_{\min, \text{toy}}$, an admissible direct remainder envelope is

$$C_{\text{SV, toy}}^{\text{op}} := 12. \quad (\text{D.41})$$

The value 12 consists of the post-quadratic and bad-denominator envelope 10 from [Lemma D.1](#), plus the exact second-order coefficient $|W_{\text{SV}}| \leq 2$ from [Equation \(D.37\)](#). This replaces the earlier worst-case envelope of order 10^7 in this specific toy. The large general constant remains a valid universal certificate, but it is not the operational constant governing this closed model.

Proposition D.3 (Two-sided finite- p SV/no-mitigation boundary). *For the toy model above, assume $p \in (0, p_{\max}]$, $16\theta^2 p_{\max}^2 \leq 1/2$, resources are restricted to $R \geq R_{\min, \text{toy}}$, and resource normalization $\kappa_0 = \kappa_{\text{SV}} = 1$. The leading SV/no-mitigation crossing*

$$R_{\text{SV} \leftrightarrow 0}(p) = \frac{s_{\text{SV}}(p) - s_0(p)}{b_0(p)^2 - b_{\text{SV}}(p)^2} \quad (\text{D.42})$$

satisfies the finite-interval sandwich

$$\frac{\varepsilon}{64\theta^2} \frac{1}{p} \leq R_{\text{SV} \leftrightarrow 0}(p) \leq \frac{8\varepsilon + 64\theta^2 p_{\max}}{\theta^2} \frac{1}{p}. \quad (\text{D.43})$$

In particular the boundary scales as $1/p$ uniformly on the declared interval.

Proof. The denominator of the crossing is $b_0(p)^2$, because $b_{\text{SV}} = 0$. The two-sided bias control is Equation (D.18). For the numerator,

$$s_{\text{SV}}(p) - s_0(p) = \frac{1}{a(p)} - (1 - \mu_0(p)^2) = \frac{1 - a(p)}{a(p)} + \mu_0(p)^2. \quad (\text{D.44})$$

Furthermore,

$$1 - a(p) = \sin^2(\theta p) + \varepsilon p \cos(2\theta p). \quad (\text{D.45})$$

Since $p \leq 1/(4|\theta|)$, $\cos(2\theta p) \geq 1/2$. Hence

$$s_{\text{SV}}(p) - s_0(p) \geq 1 - a(p) \geq \frac{\varepsilon p}{2}. \quad (\text{D.46})$$

For the upper bound, $a(p) \geq 1/2$, $\mu_0(p)^2 \leq 16\theta^2 p^2$, and

$$1 - a(p) \leq \varepsilon p + \theta^2 p^2$$

give the conservative estimate

$$s_{\text{SV}}(p) - s_0(p) \leq 4\varepsilon p + 32\theta^2 p_{\max} p. \quad (\text{D.47})$$

The constants in the last display are conservative but uniform on the declared interval. Dividing Equations (D.46) and (D.47) by the upper and lower bounds on $b_0(p)^2$, respectively, and adding one harmless factor-two slack to the lower side, gives Equation (D.43). In particular, the p -linear acceptance penalty divided by the p^2 -bias gap gives the $1/p$ boundary. \square

Proposition D.4 (Operationally non-empty certified regime for the first toy crossing). *Under the assumptions of Proposition D.3, use the direct SV toy remainder envelope $C_{\text{SV}, \text{toy}}^{\text{op}} = 12$ from Equation (D.41). The certified crossing theorem applies whenever*

$$\eta_{\text{toy}} := \frac{4C_{\text{SV}, \text{toy}}^{\text{op}}}{g(p)R_{\text{SV} \leftrightarrow 0}(p)^2} < \frac{1}{2}, \quad g(p) = b_0(p)^2. \quad (\text{D.48})$$

A sufficient parameter-level condition, using the finite-interval sandwich of Proposition D.3, is

$$\frac{32768 C_{\text{SV}, \text{toy}}^{\text{op}} \theta^2}{\varepsilon^2} < \frac{1}{2}. \quad (\text{D.49})$$

For example,

$$\varepsilon = 1, \quad |\theta| = 10^{-3}, \quad p_{\max} = 10^{-1} \quad (\text{D.50})$$

satisfy the small-angle assumptions and the certified-crossing condition, because

$$32768 \cdot 12 \cdot 10^{-6} = 3.93216 \times 10^{-1} < \frac{1}{2}. \quad (\text{D.51})$$

At the worst endpoint $p = p_{\max}$, the lower sandwich gives $R_{\text{SV} \leftrightarrow 0} \geq 1/(64 \cdot 10^{-6} \cdot 10^{-1}) > 1.5 \times 10^5$, which is safely above the fixed exponential-absorption threshold $R_{\min, \text{toy}}$. Thus the certified region is non-empty at ordinary small-noise parameters. The improvement over the earlier $\theta \sim 10^{-6}$ check comes from using the direct second-order quotient remainder in this closed toy, not from the Efron–Stein total-variance bound.

Proof. For this toy crossing, $g(p) = b_0(p)^2 - b_{\text{SV}}(p)^2 = b_0(p)^2$ and $R_0 = R_{\text{SV} \leftrightarrow 0}(p)$. The certified-crossing parameter in [Theorem 4](#) is $4C/[g(p)R_0^2]$. The sandwich bounds give $g(p) \geq \theta^2 p^2/2$ and

$$R_0 \geq \frac{\varepsilon}{64\theta^2 p}. \quad (\text{D.52})$$

Therefore

$$g(p)R_0^2 \geq \frac{\theta^2 p^2}{2} \frac{\varepsilon^2}{4096\theta^4 p^2} = \frac{\varepsilon^2}{8192\theta^2}, \quad (\text{D.53})$$

and hence

$$\eta_{\text{toy}} \leq \frac{4C \cdot 8192\theta^2}{\varepsilon^2} = \frac{32768C\theta^2}{\varepsilon^2}. \quad (\text{D.54})$$

Substituting $C = C_{\text{SV, toy}}^{\text{op}} = 12$, $\varepsilon = 1$, and $|\theta| = 10^{-3}$ proves the displayed numerical certificate. Finally, $p_{\max} = 10^{-1}$ obeys $p_{\max} \leq 1/(4\varepsilon)$ and $16\theta^2 p_{\max}^2 \ll 1/2$, so the assumptions of the finite-interval sandwich are satisfied. \square

Proposition D.5 (Selector versus Le Cam/Fisher benchmarks in the one-qubit transcript). (Conservative and sharpened versions.) *View the first toy model through the same one-qubit accepted- X -measurement transcript used in [Proposition D.1](#). Assume the certified crossing regime of [Proposition D.4](#), and restrict to the SV side of that certified crossing, i.e. budgets R larger than the certified SV/no-mitigation crossing. Then the selected leading law is*

$$\text{MSE}_{\text{sel}}^{\text{lead}}(p, R) = \frac{\text{ssv}(p)}{R} = \frac{1}{a(p)R}. \quad (\text{D.55})$$

Against the corrected conservative finite-interval Le Cam lower bound

$$L_{\text{LC}}^{\text{cons}}(p, R) = \frac{1}{32R(1-p)^2}, \quad (\text{D.56})$$

one has

$$\frac{\text{MSE}_{\text{sel}}^{\text{lead}}(p, R)}{L_{\text{LC}}^{\text{cons}}(p, R)} = \frac{32(1-p)^2}{a(p)} \leq 64. \quad (\text{D.57})$$

Using instead the local Fisher/two-point constant $I_{p, \text{loc}}^{\text{Bern}} = 2(1-p)^2$ from [Equation \(D.9\)](#), the corresponding local Le Cam scale is

$$L_{\text{LC}}^{\text{loc}}(p, R) = \frac{1}{16R(1-p)^2}, \quad (\text{D.58})$$

and therefore

$$\frac{\text{MSE}_{\text{sel}}^{\text{lead}}(p, R)}{L_{\text{LC}}^{\text{loc}}(p, R)} = \frac{16(1-p)^2}{a(p)} \leq 32. \quad (\text{D.59})$$

Finally, if the same accepted transcript is benchmarked by its regular local asymptotic Fisher information $J_{\text{acc}}(p) = a(p)$ for the accepted ideal X -mean in this toy, where SV is unbiased by construction, then the Cramer–Rao/LAN scale is

$$L_{\text{LAN}}^{\text{acc}}(p, R) = \frac{1}{a(p)R}, \quad (\text{D.60})$$

and the selected SV law saturates this accepted-transcript Fisher scale exactly. Thus the factors 64 and 32 in [Equations \(D.57\) and \(D.59\)](#) are conservative two-point artifacts, not physical evidence that the selector is far from the relevant sampling scale.

Proof. In the first toy, $\mu_{\text{SV}}(p) = \mu_{\star} = 0$, so the leading SV MSE is purely sampling and equals $s_{\text{SV}}(p)/R = 1/[a(p)R]$. The phrase “selected” is justified only on the SV side of the certified crossing supplied by [Proposition D.4](#); outside that regime the statement is only a comparison of the SV estimator, not of the selector. Dividing $1/[a(p)R]$ by the corrected conservative and local Le Cam scales gives [Equations \(D.57\) and \(D.59\)](#); $a(p) \geq 1/2$ follows from [Equation \(D.26\)](#). The number of accepted samples concentrates around $a(p)R$ by the same multiplicative Chernoff bound used in [Theorem 3](#); hence the phrase $a(p)R$ effective observations can be made high-probability rather than merely heuristic. The final LAN statement is the ordinary Fisher benchmark for those accepted unit-variance observations; it shows which part of the constant factor comes from the conservative two-point bounds. \square

Remark 12 (Role of the first toy model). *The first toy model is deliberately favorable to SV: $\delta_{\text{SV}} = 0$ because the rank-one projector kills the X -expectation inside the accepted block. Its purpose is not to prove a generic VD–SV comparison; its purpose is to show that the finite-shot crossing certificate can be checked on a finite interval with explicit constants. The next toy model gives the promised nontrivial VD–SV comparison with $\delta_{\text{SV}} \neq 0$.*

D.1 A sector toy model with $\delta_{\text{SV}} \neq 0$

The previous example has a rank-one symmetry sector, so SV has zero residual first-order bias. The present sector model is the complementary clean limit: it has nonzero SV residual bias but no dominant-eigenvector rotation, so $\delta_{\text{VD}} = 0$ at first order. These examples are deliberately diagnostic, not generic; a fully generic toy model can have both $\delta_{\text{VD}} \neq 0$ and $\delta_{\text{SV}} \neq 0$. To exhibit a genuine VD–SV boundary, consider a three-dimensional Hilbert space with orthonormal vectors $|g\rangle, |e\rangle, |\ell\rangle$. The valid sector is $P = |g\rangle\langle g| + |e\rangle\langle e|$, the ideal state is $\rho_{\star} = |g\rangle\langle g|$, and the observable is

$$O = |g\rangle\langle g| - |e\rangle\langle e|, \quad O|\ell\rangle = 0, \quad \mu_{\star} = 1. \quad (\text{D.61})$$

Let

$$\rho_p = \alpha(p)|g\rangle\langle g| + \beta(p)|e\rangle\langle e| + \lambda(p)|\ell\rangle\langle\ell|, \quad (\text{D.62})$$

with

$$\alpha(p) = 1 - (u + \ell)p, \quad \beta(p) = up, \quad \lambda(p) = \ell p, \quad (\text{D.63})$$

where $u, \ell > 0$ and $0 < p \leq p_{\text{max}} \leq [4(u + \ell)]^{-1}$. Here up is undetectable in-sector error and ℓp is detectable leakage.

SV constants. The acceptance probability and SV population value are

$$a(p) = \alpha(p) + \beta(p) = 1 - \ell p, \quad \mu_{\text{SV}}(p) = \frac{\alpha(p) - \beta(p)}{\alpha(p) + \beta(p)} = 1 - \frac{2up}{1 - \ell p}. \quad (\text{D.64})$$

Therefore

$$b_{\text{SV}}(p) = -\frac{2up}{1-\ell p}, \quad \delta_{\text{SV}} = -2u \neq 0. \quad (\text{D.65})$$

The accepted-shot variance coefficient is

$$v_{\text{SV}}(p) = \frac{1 - \mu_{\text{SV}}(p)^2}{a(p)} = \frac{4up(1 - (u + \ell)p)}{(1 - \ell p)^3} = 4up + \mathcal{O}(p^2). \quad (\text{D.66})$$

VD constants. For VD with copy number M ,

$$D_M(p) = \alpha(p)^M + \beta(p)^M + \lambda(p)^M, \quad N_M(p) = \alpha(p)^M - \beta(p)^M, \quad (\text{D.67})$$

so

$$\mu_{\text{VD},M}(p) = \frac{\alpha(p)^M - \beta(p)^M}{\alpha(p)^M + \beta(p)^M + \lambda(p)^M}. \quad (\text{D.68})$$

For $M = 2$,

$$D_2(p) = \alpha^2 + \beta^2 + \lambda^2 = 1 - 2(u + \ell)p + \mathcal{O}(p^2), \quad (\text{D.69})$$

$$N_2(p) = \alpha^2 - \beta^2 = 1 - 2(u + \ell)p + \mathcal{O}(p^2). \quad (\text{D.70})$$

A direct subtraction gives

$$b_{\text{VD},2}(p) = \frac{N_2(p)}{D_2(p)} - 1 = -\frac{2\beta(p)^2 + \lambda(p)^2}{D_2(p)} = -\frac{(2u^2 + \ell^2)p^2}{D_2(p)} = -(2u^2 + \ell^2)p^2 + \mathcal{O}(p^3), \quad (\text{D.71})$$

so VD removes the first-order in-sector error by spectral amplification. Under the independent Hadamard-test implementation of [Proposition 2](#),

$$v_{\text{VD},2}(p) = \frac{1 - N_2(p)^2 + \mu_{\text{VD},2}(p)^2(1 - D_2(p)^2)}{D_2(p)^2}, \quad (\text{D.72})$$

where the covariance term is zero because the numerator and denominator Hadamard tests are independent. Since $\mu_{\text{VD},2}(p) = 1 + \mathcal{O}(p^2)$, [Equations \(D.69\)](#) and [\(D.70\)](#) imply

$$1 - D_2(p)^2 = 4(u + \ell)p + \mathcal{O}(p^2), \quad 1 - N_2(p)^2 = 4(u + \ell)p + \mathcal{O}(p^2), \quad (\text{D.73})$$

and therefore

$$v_{\text{VD},2}(p) = 8(u + \ell)p + \mathcal{O}(p^2). \quad (\text{D.74})$$

Sector remainder and denominator certificates. On $0 < p \leq p_{\max} \leq [4(u + \ell)]^{-1}$, conservative bounded-sign moment envelopes give finite-interval certificate constants $C_{\text{VD},2}^{\text{sector}} \leq 2.5 \times 10^8$ and $C_{\text{SV}}^{\text{sector}} \leq 5.0 \times 10^7$, combined below as $C_{\text{sector}} := 3.0 \times 10^8$, together with the internal VD denominator certificate $B_{\text{den},2}(p, \varepsilon_{\text{fail}}) \leq 31 \log(2/\varepsilon_{\text{fail}})$. The full assembly, with every envelope constant displayed, is given in [Section E](#).

Proposition D.6 (Nontrivial VD–SV crossing in the sector toy). *In the sector toy, with $M = 2$ and paired-sample resource normalization $\kappa_{\text{VD},2} = \kappa_{\text{SV}} = 1$, the leading VD–SV crossing satisfies*

$$R_{\text{VD},2 \leftrightarrow \text{SV}}(p) = \frac{v_{\text{VD},2}(p) - v_{\text{SV}}(p)}{b_{\text{SV}}(p)^2 - b_{\text{VD},2}(p)^2} = \frac{u + 2\ell}{u^2} \frac{1}{p} + \mathcal{O}(1). \quad (\text{D.75})$$

Moreover, using the explicit envelope $C_{\text{sector}} = 3.0 \times 10^8$, the crossing is certified whenever

$$\eta_{\text{sector}} = \frac{4C_{\text{sector}}}{(b_{\text{SV}}^2 - b_{\text{VD},2}^2)R_{\text{VD},2\leftrightarrow\text{SV}}(p)^2} < \frac{1}{2}. \quad (\text{D.76})$$

Using the first-order bounds above, a sufficient non-empty condition is

$$\frac{8C_{\text{sector}}u^2}{(u + 2\ell)^2} < \frac{1}{2}. \quad (\text{D.77})$$

The internal VD quotient certificate is simultaneously valid if, with the chosen resource normalization,

$$\frac{u + 2\ell}{u^2 p_{\text{max}}} \geq 31 \log \frac{2}{\varepsilon_{\text{fail}}}. \quad (\text{D.78})$$

For example, $u = 1$, $\ell = 10^6$, $p_{\text{max}} = 10^{-8}$, and $\varepsilon_{\text{fail}} = 10^{-6}$ satisfy both [Equations \(D.77\)](#) and [\(D.78\)](#). This numerical point is deliberately extreme: $\ell/u = 10^6$ and $p_{\text{max}} = 10^{-8}$ do not represent a realistic device regime. They only demonstrate that the nested certificates are jointly non-empty under the conservative constants of [Remark 1](#). Sharper variance remainders would move the certified example toward much less extreme parameter ratios. Hence the VD–SV crossing certificate and the internal VD denominator certificate are jointly non-empty.

Proof. [Equations \(D.65\)](#) and [\(D.71\)](#) give $b_{\text{SV}}(p)^2 - b_{\text{VD},2}(p)^2 = 4u^2p^2 + \mathcal{O}(p^3)$. [Equations \(D.66\)](#) and [\(D.74\)](#) give $v_{\text{VD},2}(p) - v_{\text{SV}}(p) = (4u + 8\ell)p + \mathcal{O}(p^2)$. Dividing proves [Equation \(D.75\)](#). The certified condition is exactly [Equation \(97\)](#) with the explicit sector-toy constants from [Equation \(E.9\)](#). Substituting the leading lower bound $b_{\text{SV}}^2 - b_{\text{VD},2}^2 \geq 2u^2p^2$ and the crossing lower bound $R_{\text{VD},2\leftrightarrow\text{SV}} \geq (u + 2\ell)/(2u^2p)$ for small enough p_{max} yields [Equation \(D.77\)](#). The separate lower bound [Equation \(D.78\)](#) is just $R_{\text{cross}}(p_{\text{max}}) \geq B_{\text{den},2}$, using [Equation \(E.10\)](#). The displayed numerical choice verifies both inequalities directly. \square

Proposition D.7 (Efron–Stein total-MSE dominance check at physical noise). *The extreme numerical point in [Proposition D.6](#) is not needed to obtain an operationally meaningful dominance certificate. In the sector toy with*

$$u = 1, \quad \ell = 1, \quad p = 10^{-2}, \quad M = 2, \quad (\text{D.79})$$

and unit Hadamard-test call costs, let R denote the physical call budget. Since the independent VD implementation uses one numerator and one denominator stream, its paired-shot budget is $B = R/2$. The clipped VD estimator is certified to beat SV at any physical budget

$$R \geq 2 \times 10^6. \quad (\text{D.80})$$

More precisely, the Efron–Stein total-variance certificate gives

$$\text{Var}(\hat{\mu}_{\text{VD},2}^{\text{clip}}) \leq \frac{472}{R}, \quad (\text{D.81})$$

while the VD population bias satisfies

$$|b_{\text{VD},2}(p)| \leq 4p^2, \quad (\text{D.82})$$

and the SV residual floor satisfies, with $\varepsilon_{\text{SV},\text{sector}}^{(E)}(R)$ denoting the explicit SV expectation-remainder bound from [Theorem 3](#),

$$\text{MSE}_{\text{SV}}(p, R) \geq \left(|b_{\text{SV}}(p)| - \varepsilon_{\text{SV},\text{sector}}^{(E)}(R) \right)^2 \geq 4p^2. \quad (\text{D.83})$$

Consequently, at $p = 10^{-2}$ and $R = 2 \times 10^6$,

$$\text{MSE}_{\text{VD},2}^{\text{cert}}(p, R) \leq (4p^2 + 4/R)^2 + \frac{472}{R} + 10^{-8} < 2.4 \times 10^{-4} < 4.0 \times 10^{-4} \leq \text{MSE}_{\text{SV}}(p, R). \quad (\text{D.84})$$

Thus VD can be certified to beat SV in total MSE at a physical noise scale using modest sector ratios. This is not a replacement for the crossing-remainder certificate in [Theorem 4](#): Efron–Stein controls the total variance of the clipped quotient, not the difference between the exact MSE and its leading local law. It is included only as a robust dominance check showing that the extreme constants in the formal crossing certificate are not physical thresholds.

The proof is a direct numerical verification of each displayed bound and is given in [Section C](#).

Proposition D.8 (Sector residual-bias floor and a structural two-point benchmark). *In the sector toy, SV has residual first-order bias*

$$b_{\text{SV}}(p) = -2up + O(p^2), \quad b_{\text{SV}}(p)^2 = 4u^2p^2 + O(p^3). \quad (\text{D.85})$$

Consider the restricted ambiguity model in which the same full noisy state ρ_p can be generated either from the ideal state $\rho_+^* = |g\rangle\langle g|$ with an undetectable in-sector error of mass up , or from an alternative ideal state $\rho_-^* = (1 - up)|g\rangle\langle g| + up|e\rangle\langle e|$ with that in-sector mass treated as ideal population, with the remaining channel adjusted so that the transcript distribution is identical. The two ideal values differ by

$$\mu_+^* - \mu_-^* = 2up. \quad (\text{D.86})$$

Hence [Corollary 3](#) gives the structural lower bound

$$L_{\text{str}}^{\text{sector}}(p) = \frac{u^2p^2}{2}. \quad (\text{D.87})$$

Consequently the SV residual bias floor is within a constant factor of this restricted non-identifiability floor:

$$\frac{b_{\text{SV}}(p)^2}{L_{\text{str}}^{\text{sector}}(p)} = 8 + O(p). \quad (\text{D.88})$$

This does not say that VD cannot beat SV in the declared known-channel sector model; VD does beat SV on the high-budget side of [Proposition D.6](#). It says something narrower: if the in-sector population error is not identifiable from side information, then the same order of bias floor is information-theoretic rather than merely a defect of SV.

Proof. The expansion of b_{SV} is [Equation \(D.65\)](#). The two hypotheses described in the statement induce the same noisy transcript distribution by construction, while their ideal $O = |g\rangle\langle g| - |e\rangle\langle e|$ values are 1 and $1 - 2up$. Applying [Corollary 3](#) with $h = up$ gives [Equation \(D.87\)](#). Dividing the SV squared bias by this floor gives [Equation \(D.88\)](#). \square

Remark 13 (Role of the sector toy model). *The sector toy is favorable to VD by construction, complementing the first toy’s design in favor of SV. Because ρ_p remains diagonal in the fixed basis $\{|g\rangle, |e\rangle, |\ell\rangle\}$, the dominant eigenvector does not rotate and $\delta_{\text{VD}} = 0$. Its purpose is to isolate the spectral-amplification advantage of VD against a nonzero SV residual bias. The generic operating-window theory above allows both $\delta_{\text{VD}} \neq 0$ and $\delta_{\text{SV}} \neq 0$; these two closed models are diagnostic boundary cases used to check constants, not a claim that either favorable limit is typical.*

D.2 A generic toy with simultaneous VD and SV first-order bias

The two closed toy models above isolate clean limiting mechanisms. The first makes SV unbiased at first order; the sector model removes dominant-eigenvector rotation and therefore gives $\delta_{\text{VD}} = 0$. The following minimal model records the generic situation in which both first-order floors can be nonzero. It is included as a structural diagnostic only. The direct trace expansion and the formal VD–SV crossing are displayed below; only the sharp variance constants and a full certified-boundary check for this generic non-diagonal toy are left for future work.

Proposition D.9 (A toy with simultaneous VD and SV first-order bias). *Work in \mathbb{C}^3 with basis $\{|0\rangle, |1\rangle, |2\rangle\}$, valid sector*

$$P = |0\rangle\langle 0| + |1\rangle\langle 1|, \quad (\text{D.89})$$

ideal state $\rho_\star = |0\rangle\langle 0|$, and observable

$$O = |0\rangle\langle 0| - |1\rangle\langle 1| + c(|0\rangle\langle 1| + |1\rangle\langle 0|), \quad \mu_\star = 1. \quad (\text{D.90})$$

Let

$$\Delta = u(|1\rangle\langle 1| - |0\rangle\langle 0|) + \ell(|2\rangle\langle 2| - |0\rangle\langle 0|) + \kappa(|0\rangle\langle 1| + |1\rangle\langle 0|), \quad u, \ell, \kappa > 0, \quad (\text{D.91})$$

and set $\rho_p = \rho_\star + p\Delta$ for

$$0 < p \leq p_0, \quad p_0 := \frac{1}{2} \min \left\{ \frac{1}{u + \ell}, \frac{u}{\kappa^2} \right\}. \quad (\text{D.92})$$

Then ρ_p is a density matrix on this interval. Its trace is one, its $|2\rangle$ weight is $\ell p \geq 0$, and the $\{|0\rangle, |1\rangle\}$ block has determinant

$$p[u - (u(u + \ell) + \kappa^2)p] \geq 0 \quad (\text{D.93})$$

by [Equation \(D.92\)](#). Here up is an undetectable in-sector population error, ℓp is detectable leakage, and κp is an in-sector coherence that tilts the dominant eigenvector. Then

$$a(p) = 1 - \ell p, \quad \delta_{\text{SV}} = 2(c\kappa - u), \quad \delta_{\text{VD}} = 2c\kappa. \quad (\text{D.94})$$

Thus, whenever $c\kappa \neq 0$ and $c\kappa \neq u$, both VD and SV have nonzero first-order residual bias. For $M = 2$, direct trace expansion gives

$$D_2(p) = \text{Tr}(\rho_p^2) = 1 - 2(u + \ell)p + \mathcal{O}(p^2), \quad (\text{D.95})$$

$$N_2(p) = \text{Tr}(O\rho_p^2) = 1 + 2(c\kappa - u - \ell)p + \mathcal{O}(p^2), \quad (\text{D.96})$$

and hence

$$b_{\text{VD},2}(p) = 2c\kappa p + \mathcal{O}(p^2), \quad b_{\text{SV}}(p) = 2(c\kappa - u)p + \mathcal{O}(p^2). \quad (\text{D.97})$$

Writing the leading sampling coefficients as

$$s_{\text{VD},2}(p) = \nu_{\text{VD},0} + \mathcal{O}(p), \quad s_{\text{SV}}(p) = \nu_{\text{SV},0} + \mathcal{O}(p), \quad (\text{D.98})$$

the formal VD–SV crossing in the generic toy is

$$R_{\text{VD},2 \leftrightarrow \text{SV}}(p) = \frac{\nu_{\text{VD},0} - \nu_{\text{SV},0} + \mathcal{O}(p)}{4[(c\kappa - u)^2 - c^2\kappa^2]p^2 + \mathcal{O}(p^3)}, \quad (\text{D.99})$$

whenever the denominator is nonzero and the numerator has the sign required for a positive crossing. For the natural scaled-Hadamard VD numerator and eigenbasis SV measurement in this toy, the matched per-sample constants are equal at $p = 0$: $\nu_{\text{VD},0} = \nu_{\text{SV},0} = c^2$. Hence matched per-sample normalization gives $\nu_{\text{VD},0} - \nu_{\text{SV},0} = 0$ and the leading window reverts to $\Theta(p^{-1})$ if the $O(p)$ sampling coefficients differ. Under physical-call normalization for independent VD, however, $\kappa_{\text{VD},2} = 2\kappa_{\text{SV}}$, so the resource-normalized constants are $2c^2$ versus c^2 . When $c \neq 0$ and the bias-gap denominator in [Equation \(D.99\)](#) is nonzero, [Corollary 1](#) then gives the usual $\Theta(p^{-2})$ window. The exponent is therefore an implementation-and-resource-normalization statement, not a property of simultaneous first-order bias alone.

Proof. Since $\text{Tr}(P\Delta P) = \Delta_{00} + \Delta_{11} = -(u + \ell) + u = -\ell$, the acceptance probability is exactly $a(p) = 1 - \ell p$. Also

$$\text{Tr}(OP\Delta P) = O_{00}\Delta_{00} + O_{11}\Delta_{11} + 2c\Delta_{01} = -(u + \ell) - u + 2c\kappa. \quad (\text{D.100})$$

Using the first-order SV formula gives

$$\delta_{\text{SV}} = \text{Tr}(OP\Delta P) - \mu_{\star} \text{Tr}(P\Delta P) = -(2u + \ell) + 2c\kappa + \ell = 2(c\kappa - u). \quad (\text{D.101})$$

For VD, let $Q_{\star} = I - |0\rangle\langle 0|$. Then $\Delta|0\rangle = -(u + \ell)|0\rangle + \kappa|1\rangle$, so $Q_{\star}\Delta|0\rangle = \kappa|1\rangle$. By [Proposition 1](#),

$$\delta_{\text{VD}} = 2\Re\langle 0|OQ_{\star}\Delta|0\rangle = 2c\kappa. \quad (\text{D.102})$$

Finally, $\rho_p = \rho_{\star} + p\Delta$ on the declared positivity interval gives

$$\rho_p^2 = \rho_{\star} + p(\rho_{\star}\Delta + \Delta\rho_{\star}) + \mathcal{O}(p^2). \quad (\text{D.103})$$

Since $\text{Tr}(\rho_{\star}\Delta + \Delta\rho_{\star}) = 2\Delta_{00} = -2(u + \ell)$, [Equation \(D.95\)](#) follows. Also

$$\text{Tr}[O(\rho_{\star}\Delta + \Delta\rho_{\star})] = -2(u + \ell) + 2c\kappa, \quad (\text{D.104})$$

which gives [Equation \(D.96\)](#). Dividing N_2/D_2 yields $b_{\text{VD},2} = 2c\kappa p + \mathcal{O}(p^2)$. Combining this with the SV expansion above and equating the two leading MSE laws gives [Equation \(D.99\)](#). \square

Remark 14 (Why the previous clean toys were special). *The first toy is SV-favorable because the postselected observable has zero residual first-order bias. The sector toy is VD-favorable because the noisy state is diagonal in a fixed basis, so the dominant eigenvector does not rotate at first order. [Proposition D.9](#) shows that neither simplification is generic: an in-sector coherence can make $\delta_{\text{VD}} \neq 0$, and an undetectable in-sector population error can make $\delta_{\text{SV}} \neq 0$. In particular, a diagonal observable in the ideal eigenbasis has $\delta_{\text{VD}} = 0$ because it cannot see the orthogonal first-order tilt direction $Q_{\star}\Delta|\psi_{\star}\rangle$; off-diagonal observables generally can. This is the same regime dependence seen in the QAOA validation layer: the clean sector toy is VD-favorable by construction, whereas the realistic QAOA circuits are SV-favorable once Hadamard/SWAP, controlled-SWAP, routing, and readout overhead are included. These are not contradictory outcomes; they are different points in the operating-window landscape, and the absence of a universal winner is part of the claim.*

E Toy-model certificate arithmetic

This appendix displays the conservative envelope arithmetic behind the sector-toy certificate constants used in [Propositions D.6](#) and [D.7](#).

Sector remainder and denominator certificates. On $0 < p \leq p_{\max} \leq [4(u + \ell)]^{-1}$, one has $\alpha(p) \geq 3/4$ and hence

$$D_2(p) = \alpha^2 + \beta^2 + \lambda^2 \geq \frac{9}{16}, \quad a(p) = 1 - \ell p \geq \frac{3}{4}. \quad (\text{E.1})$$

For the independent Hadamard-test VD implementation with $M = 2$, take $K_{N,2} = 1$, $K_{D,2} = 2$, and the bounded-moment envelopes

$$\mathbf{m}_{12}, \mathbf{m}_{21}, \mathbf{m}_{03} \leq 8, \quad \mathbf{m}_{13}, \mathbf{m}_{04}, \mathbf{m}_{22}, \mathbf{m}_{40} \leq 64, \quad \mathbf{t}^{(V)} \leq 10^6. \quad (\text{E.2})$$

The final bound on $\mathbf{t}^{(V)}$ is a direct bounded-sign envelope for the third-and-higher quotient terms in this finite sector toy; it is loose by construction and remains far below the conservative crossing constant used below. The finite-interval constant is assembled explicitly as follows. Let $\Delta = (9/16)^{-1} = 16/9$. Since $D_2^{-1} \leq \Delta$ and $|\mu_{\text{VD},2}| \leq 1$, Equation (B.8) gives

$$A_{E,\text{VD},2}^{\text{sector}} \leq (8 + 8)\Delta^3 + 64\Delta^4 + 2 \cdot 1 \cdot 64\Delta^5 \quad (\text{E.3})$$

$$< 3.1 \times 10^3. \quad (\text{E.4})$$

Using the same envelopes in Equations (B.9) to (B.11),

$$A_{V,\text{VD},2}^{\text{sector}} \leq 2\Delta^4(64 + 64) + 2\Delta^3(2 \cdot 8 + 8 + 8) + 10^6 \quad (\text{E.5})$$

$$< 1.1 \times 10^6 < 2.5 \times 10^8. \quad (\text{E.6})$$

In the MSE remainder assembly, the dominant displayed correction is the quadratic envelope $2(A_{E,\text{VD},2}^{\text{sector}})^2 < 2.0 \times 10^7$; the additional A_V , c^2 , $2|b|A_E$, and $2|c|A_E$ terms are smaller on the declared finite interval. This justifies the stated conservative finite-interval bound

$$C_{\text{VD},2}^{\text{sector}} \leq 2.5 \times 10^8. \quad (\text{E.7})$$

For SV in the sector toy, $a \geq 3/4$, $K_W = 1$, and the Bernoulli quotient constants give

$$C_{\text{SV}}^{\text{sector}} \leq 5.0 \times 10^7. \quad (\text{E.8})$$

This SV bound is similarly conservative; inserting $a \geq 3/4$ in the explicit constants of Theorem 3 gives a value far below 5.0×10^7 , and the larger number is retained only to keep a simple round sector envelope. We therefore use the explicit envelope

$$C_{\text{sector}} := 3.0 \times 10^8. \quad (\text{E.9})$$

The internal VD denominator certificate is also explicit. Since $\sigma_{D,2}^2 \leq 1$, $K_{D,2} = 2$, and $D_2 \geq 9/16$, Equation (30) gives

$$B_{\text{den},2}(p, \varepsilon_{\text{fail}}) \leq 31 \log \frac{2}{\varepsilon_{\text{fail}}}. \quad (\text{E.10})$$

Thus the VD law used inside the crossing is certified whenever the VD sample budget at the predicted crossing is at least the right-hand side of Equation (E.10).

F Notation map

Symbol	Meaning
p	Physical noise scale
B	Statistical sample count for one method
R	Common physical resource budget after method-specific cost normalization
ρ_\star	Ideal output state
ρ_p	Noisy output state
$\Delta = \mathcal{L}(\rho_\star)$	First-order noise perturbation
O	Observable
μ_\star	Ideal expectation value
D_M	VD denominator $\text{Tr}(\rho_p^M)$
$b_m(p)$	Population residual bias of method m
$c_m(p)$	Statistical quotient-bias coefficient
$\rho_m(p, B), \rho_m(p, R)$	Certified B^{-2} or R^{-2} local-law remainder, not a quantum state
$\gamma_m(p), \gamma_{\text{VD},M}(p)$	Exponential bad-event rate in certified local-law remainders
$\gamma(p)$	PEC quasiprobability one-norm overhead, not an exponential concentration rate
$s_m(p)$	Resource-normalized sampling coefficient
$\omega_M = K_{D,M}/D_M$	Denominator-size ratio used only in quotient-remainder prefactors
κ_m, κ_M	Resource cost per method sample, or per Hadamard test for copy number M
$a(p)$	SV acceptance probability
δ_{VD}	VD dominant-eigenvector mismatch coefficient
δ_{SV}	SV undetectable-sector bias coefficient